Journal of
Composites Science

MDPI

Review

Fused Deposition Modelling of Fibre Reinforced Polymer Composites: A Parametric Review

Narongkorn Krajangsawasdi *, Lourens G. Blok, Ian Hamerton, Marco L. Longana, Benjamin K. S. Woods and Dmitry S. Ivanov

Department of Aerospace Engineering, Bristol Composites Institute (ACCIS), Queen's Building, University of Bristol, University Walk, Bristol BS8 1TR, UK; lourens.blok@bristol.ac.uk (L.G.B.); ian.hamerton@bristol.ac.uk (I.H.); m.l.longana@bristol.ac.uk (M.L.L.); ben.k.s.woods@bristol.ac.uk (B.K.S.W.); dmitry.ivanov@bristol.ac.uk (D.S.I.)

* Correspondence: ih18506@bristol.ac.uk

Abstract: Fused deposition modelling (FDM) is a widely used additive layer manufacturing process that deposits thermoplastic material layer-by-layer to produce complex geometries within a short time. Increasingly, fibres are being used to reinforce thermoplastic filaments to improve mechanical performance. This paper reviews the available literature on fibre reinforced FDM to investigate how the mechanical, physical, and thermal properties of 3D-printed fibre reinforced thermoplastic composite materials are affected by printing parameters (e.g., printing speed, temperature, building principle, etc.) and constitutive materials properties, i.e., polymeric matrices, reinforcements, and additional materials. In particular, the reinforcement fibres are categorized in this review considering the different available types (e.g., carbon, glass, aramid, and natural), and obtainable architectures divided accordingly to the fibre length (nano, short, and continuous). The review attempts to distil the optimum processing parameters that could be deduced from across different studies by presenting graphically the relationship between process parameters and properties. This publication benefits the material developer who is investigating the process parameters to optimize the printing parameters of novel materials or looking for a good constituent combination to produce composite FDM filaments, thus helping to reduce material wastage and experimental time.

Keywords: fused deposition modelling; thermoplastics; fibre reinforced thermoplastic; parametric study

Citation: Krajangsawasdi, N.; Blok, L.G.; Hamerton, I.; Longana, M.L.; Woods, B.K.S.; Ivanov, D.S. Fused Deposition Modelling of Fibre Reinforced Polymer Composites: A Parametric Review. *J. Compos. Sci.* **2021**, *5*, 29. https://doi.org/10.3390/jcs5010029

Received: 9 December 2020
Accepted: 12 January 2021
Published: 16 January 2021

1. Introduction

Additive layer manufacturing (ALM) fabricates objects from a three-dimensional (3D), computer-aided design (CAD) model by stacking material in a layer-by-layer arrangement [1]. ALM, as a layer-based manufacturing method, allows to fabricate complex geometries within a short time compared to conventional subtractive manufacturing methods, so it is also known as rapid prototyping [2,3]. The reduction in design limitations shortens the design and manufacturing cycle whilst speeds up the development process that leads to high-efficiency products, especially for mass-customized items [4,5]. ALM is also cost-effective as it minimises additional expenses such as those associated with tooling or moulds. The higher degree of automation of ALM can reduce human error and increase product accuracy. After the invention of the first ALM methods, laser-based and photochemical stereolithography (SLA) [2], various other approaches based on layer manufacturing were developed, for instance, selective laser sintering (SLS), powder bed and inkjet head 3D printing (3DP), etc. [6,7].

Among the several ALM methods, one of the most widespread [8,9], is a polymer fused deposition technique also known as variably as Fused Deposition Modelling (FDM) [7], Fused Filament Fabrication (FFF) [10], Solid Filament Freeform (SFF) [6,11], or Material Extrusion Additive Manufacturing (MEAM) [12]. In this paper, it will be referred to as

FDM or 3D printing. The reasons for its popularity compared to other ALM methods are immediate: ease of use [13] and no extra equipment required (e.g., mould, oven, or tools) [2,14,15], leading to low costs of machines and processes. Typically, raw materials for FDM are thermoplastics in the form of solid feedstock, which are of low toxicity and are easy and safe to handle during processing [16,17]. Besides, the nature of thermoplastics, which can be heated and reshaped, allows the products to be recyclable [18,19]. FDM was first developed by S. Scott Crump, co-founder of Stratasys, in 1988 [20–23] and generally, the process starts with generating a 3D CAD model and transforming it into a generic geometry file (typically an STL file). This geometry file is then "sliced" using one of the many open-source or proprietary slicing software, which cut the geometry into a series of layers and encode the machine commands (position, temperature, etc.) into a G-code file readable by the FDM machine [20,21,24].

In the machine, a thermoplastic feedstock is fed into a melt pool where it is heated until it reaches a melted state above its glass transition temperature (T_g) [25], it is finally extruded through a fine tip nozzle [12,16,25]. The deposited filaments, called rasters (roads lines or beads), are placed side by side in the horizontal (XY) plane to build a layer. When the first layer is built on the printed bed, the material is deposited on top of the previous raster in the through-thickness direction. The relative movement of the extrusion head and printing bed is defined by computer numeric controls (CNC) [2,24]. The adjacent deposited rasters fuse together and become a solid part after cooling down [26]. Sometimes, overhung sections of the geometry need support structures, which are usually made from removable materials (via a second nozzle) or perforated junctions [27]. The nature of layer-by-layer and plastic fusion makes the part highly anisotropic [26–28]. Hence, the strength depends mainly on the process parameters to achieve good raster fusion and the mechanical performance of the thermoplastic material itself. The defects, such as the voids between rasters, can be minimized by optimising the printing parameters and the fusion of the deposition can be strengthened [21,29]; moreover, the dimensional accuracy can be maximized by decreasing die swelling or edge shrinking [8,16,30].

The process is restricted only to those thermoplastics, of which the most common are listed below, that can be processed in at easily achievable temperatures, i.e., below 300 °C. Most of the commonly used thermoplastics in the FDM are low-end thermoplastics with low thermal properties, i.e., low T_g, melting temperature (T_m), high tendency to shrink during solidification, etc., and low mechanical performance compared to thermosetting polymers or metals. This usually limits the use of the product to only prototypes. Examples of low-end FDM thermoplastics are polypropylene (PP), poly(acrylonitrile-butadiene-styrene) (ABS), poly(lactic acid) (PLA), polycarbonate (PC), polyamide (PA, nylon) which have low to intermediate thermal and mechanical properties for general applications [12,25,31,32]. To increase the mechanical performance for manufacturing of functional products, high-end thermoplastics such as poly(ether ether ketone) (PEEK) or polyetherimide (PEI, ULTEM1000) can be selected but they require higher process temperature, i.e., up to 350 °C, achievable only with special high-temperature machines, high performance heater and heat protection [16,17,33].

To improve the low material properties of the common thermoplastics, the composite concept, i.e., the reinforcement of the polymeric feedstock with a second phase, was introduced to FDM [1,15,19,29]. Various types of fillers have been blended to the polymeric matrix to improve both mechanical and thermal properties. The first application capable of exploiting the high mechanical performance and manufacturability offered by fibre reinforced FDM was the manufacturing of an aerofoil for an aircraft wing building feasibility study [34,35]. Subsequently, more complex structures, which are time-consuming with conventional manufacturing processes, such as a truss structure for airframe fuselage of a drone [36] or honeycomb structure [19,37], were experimentally studied. Among the studies of the fibre reinforcement in FDM, the critical fibre length, which strongly affects the strength of short fibre composite, has not been considered extensively in the

available literature. In addition, the different filament-forming methods for different fibre architectures have rarely been reviewed.

As an attempt to expand the application of the FDM product, printing procedures to strengthen the product or novel FDM materials, especially fibre reinforced thermoplastics, have been invented and studied to improve performance of the available FDM products. This paper gathers articles relating with FDM process, mainly experimental based study, and then describes the effect of printing and material parameters on the mechanical, physical, and thermal properties of FDM manufactured parts by dividing into two sections. Section 2 describes the FDM process parameters that relate to the setup values during G-code generation. The relationship between process parameters and the mechanical performance is shown graphically to provide a guideline to optimize the process parameters that can reduce trial and error iteration for the material developer resulting in faster R&D and less material wastage. Section 3 is the material parameter part that describes the various types of thermoplastics, reinforcements focusing on various types, e.g., carbon fibre (CF), glass fibre (GF), and *para*-aramid fibre (Kevlar fibre, KF), and architectures divided accordingly to the fibre length, e.g., nano, short, and continuous, of fibres, and additional materials. Then, the FDM composite performance will be analysed at different structure scale from microstructure (i.e., fibre, matrix, and their interactions) to mesostructured (the sintering between the printed rasters, inter-raster bonding) and then the overall structure (i.e., the finished part) in order to determine the composite performance and understand the optimum solution to reinforce the FDM thermoplastic. Parameters and properties achieved, considered in this review, are illustrated in Figure 1. The overall study of printing and material parameters in the quoted articles are shown in Tables A1–A3 in Appendix A which is organised according to the composition of the filament: neat thermoplastic, short/discontinuous fibre, and continuous fibre, respectively. The main examined property, i.e., tensile stiffness and strength of each study are illustrated in Tables A1–A3.

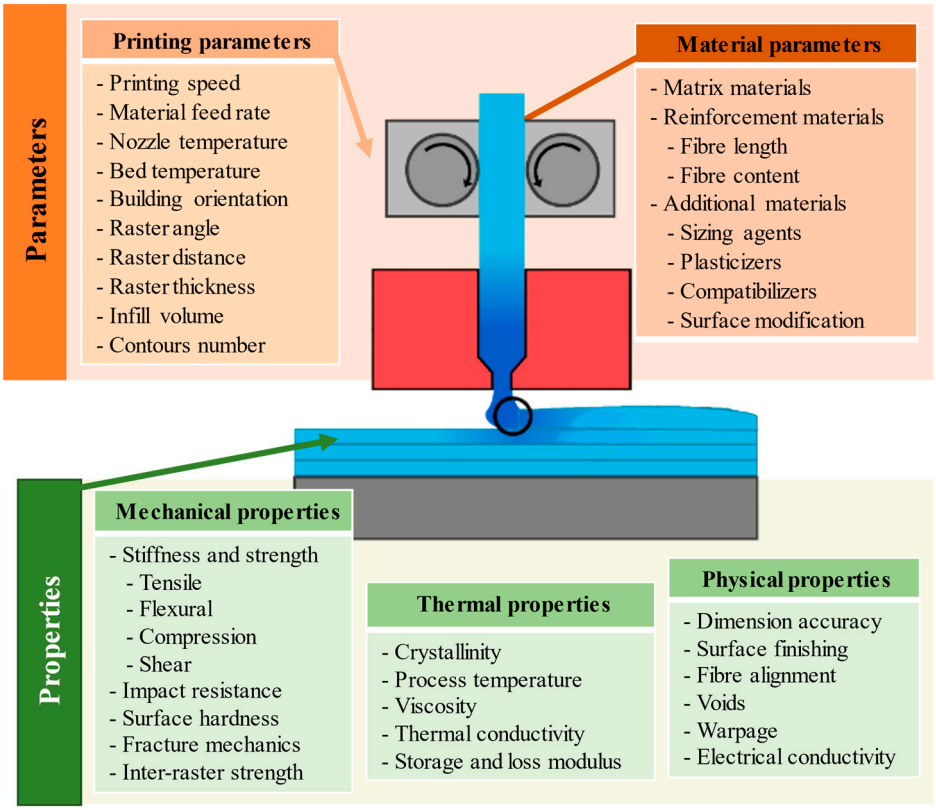

Figure 1. Investigated parameters and properties of the fused deposition modelling (FDM) process.

2. Printing Parameters

This section describes the adjustable parameters in the FDM process and their influence on mechanical, thermal, and physical properties, as detailed in Figure 1. Tensile strength, the main study property, is shown graphically as a function of several independent printing parameters. Furthermore, other dependent variables, e.g., viscosity and crystallinity, are described to give an idea of the optimum printing parameters. The main focus is on the fibre reinforced thermoplastic FDM products. In some printing parameters, there are a few studies on fibre reinforced thermoplastics. Thus, the neat polymer studies are also mentioned to understand the FDM process and products behaviour that can be applied to develop FDM with fibre reinforced plastics.

2.1. Printing Speed

Printing speed is the velocity of the nozzle in the XY plane to fill the sliced layer and in the vertical (Z) direction when finishing a layer. In most of the commercially available devices, it is controlled by a series of stepper motors connected to screws or conveyor belts. The speed can be assigned in the G-code, its unit usually is mm/min. The printing speed affects the part strength, manufacturing time, and part appearance [23]. It influences the neat polymer printed part internal structure i.e., internal porosity and interlayer bonding.

At high printing speeds, the inter-raster bonding period is limited resulting in a weak interlayer bonding and porosity. Moreover, for thermoplastic reinforced fibre materials, high printing speed shortens the fibre–matrix impregnation time resulting in poor fibre–matrix interaction [38]. Consequently, printing at high speed causes lower tensile, flexural and shear properties than printing at the low speed [4,27,35,39]. Moreover, the high speed shortens the cooling time before deposition of the next layer and leave a high amount of material at a high temperature. The high temperature material may help the raster fusion but leaving the thermoplastic at high temperature for a long period can cause sagging of the material due to gravity. The sagging changes the printed part dimension and so it can hinder the continuous printing process as detailed by Brenken et al. [40]. The printing speed also affects the dimensional accuracy of a part. A low printing speed slowly moves the nozzle, so the deposited rasters are steadily placed on top of the previous layer, allowing for more ordered raster and higher accuracy [23]. The pressure drop that controls the melt flow is affected by the speed described in Geng et al. [16] study on PEEK 3D printing. The too low speed (<65 mm/min) caused insufficient pressure-drop to spread the melt flow material and too high printing speed (>400 mm/min) resulted in material slippage. Both cases reduced the raster width.

In some G-code generators, the printing speed of the first layer, i.e., the one in contact with the printing bed, can be assigned differently from other layers and the first layer speed is normally set to be lower than the rest. This can be justified by the fact that a lower printing speed for the first layer may improve adhesion of the material to the bed, due to the higher time for compaction, i.e., the pressure applied by the nozzle to the material. To reduce the printing time, the printing speed can be increased for printing the plastic on to plastic, in the following layers, that can fuse together more easily than plastic to bed [12,19,41].

Figure 2 shows the influence of speed used in various publications with a wide array of materials on the tensile strength (■, ✻, and ▲ refer to neat thermoplastic, short and continuous fibre reinforced plastic, respectively). It is obvious that the continuous fibre reinforcement materials used lower speed (<600 mm/min) while the short fibre reinforcement and neat thermoplastic materials were deposited at higher speeds (up to 3600 mm/min). Comparing the speed in the same studies, shown as data points linked by a continuous line in Figure 2, the higher printing speed slightly reduces the tensile strength, but the printing speed has a limited effect compared to the tensile strength of different materials used.

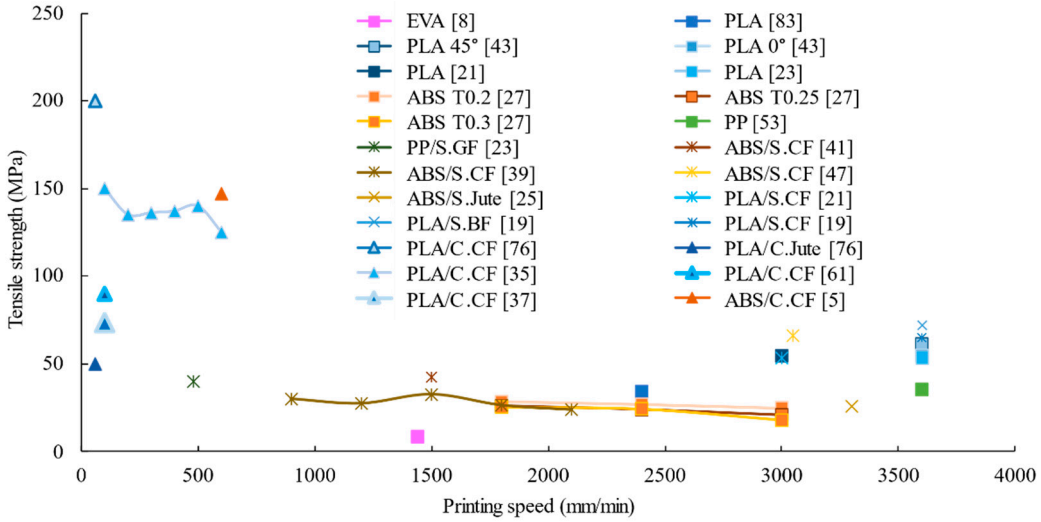

Figure 2. Tensile strength at different speed of different materials (the information gathered from several studies shown in Appendix A Tables A1–A3).

2.2. Material Feed Rate or Extrusion Rate

The feed rate or extrusion rate is the velocity at which the solid filament is fed to the heated nozzle; it is controlled by a stepper motor connected to a roller with a grooved, toothed, or gear-like surface that grips the filament by friction and pushes it to the hot-end. This velocity controls the amount of material in the heated nozzle that controls the pressure drop, reduction pressure along with the convergence printing nozzle following Bernoulli's principle, pushing the melted material out from the nozzle. The feed rate needs to match with the T_g and T_m to achieve the proper melting and extrusion. The feed rate (FR) can be calculated from the material flow rate (Q) and the expected dimension of the printed raster (width (W) and height (H)) or the angular velocity of the feeder motor (ω) and the feeder roller radius (R_f) using Equation (1)

$$FR = \frac{Q}{W \times H} = \omega R_f \tag{1}$$

The maximum force (F_{max}) to drive the filament to the nozzle is limited by buckling of the filament according to critical force (P_{cr}) in Euler's bucking equation (Equation (2))

$$F_{\max} = P_{cr} = \frac{\pi^2 E D^2}{16 L_f^2} \tag{2}$$

where E is the elastic modulus of the filament, D is the solid filament diameter, and L_f is the filament length from the rollers to the entrance of the liquefier. At high feed rate, the high amount of material fed to the liquefier leads to high melted pressure and high pressure drop [42]. This reduces expansion and bubble generation in the material, so the surface defects are minimized [16,42]. However, the too high feed rate, over 80 mm/min observed by Geng et al. [16], may cause an excessive melting pressure resulting in insufficient power and the melt flows upward along the gap between the nozzle wall and the convergence zone in the nozzle, blocking the nozzle. The print speed and feed rate need to be synchronized to avoid unstable dimensions of the printed part. The printing speed (PS) and feed rate have a relationship following Equation (3):

$$\frac{PS}{FR} = \left(\frac{D}{d}\right)^2 \tag{3}$$

where *d* is the diameter of the nozzle [16]. For continuous fibre reinforced plastics, formed using a co-extrusion method, the synchronisation between the feed rate and deposition speed is the key control of the fibre content especially in the separate fibre and matrix printing systems (described below in Section 3.2.1).

For pre-impregnated continuous fibre reinforced plastic, the feed rate of fibre and deposition speed of the printed composite should be set at the same value. If the printing speed is higher than the feed rate, the fibre will be pulled causing residual tensile stress in the fibre and it may cause them to be torn apart or broken. By contrast, a printing speed lower than the feed rate is expected to result in the fibre wrinkle or nozzle clogging by the excessive material.

2.3. Nozzle Temperature

This is the material extrusion temperature driven by an active response heater commanded with the printer controller. The temperature relates to the T_g and T_m of the printing materials. It usually set above the T_g to allow the material to soften and fuse to the previously deposited rasters, but below the degradation temperature ($T_{5\%}$) to avoid property changing. The nozzle temperature affects the chemical structure of polymers. A high nozzle temperature increases the crystallinity of the printed rasters, this can increase the tensile strength [8,43]. A series of research [39,40,43], suggested that the high temperature also heated the previously deposited material, this, in combination with the residual heat of the currently deposited raster enhanced the raster fusion as seen in the raster temperature distribution in Figure 3a. A better fusion and low viscosity at high temperature allow the adjacent deposited rasters to sinter to each other. When the rasters are completely welded, the polymer chains are intermingled and they form a randomized chain in the fusion structure (the process is shown in Figure 3b–e) reflecting into good inter-raster-bonding strength of the part [44].

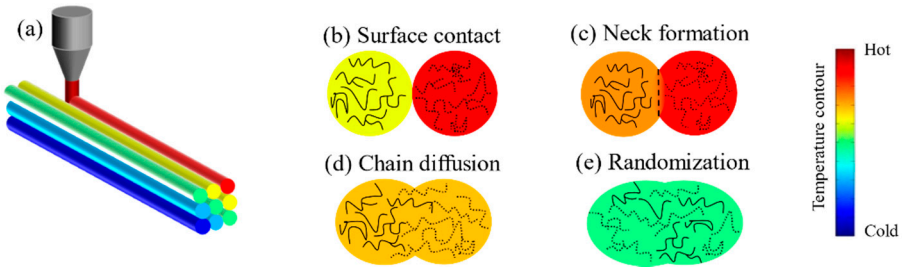

Figure 3. (**a**) Temperature distribution of the printed rasters from the highest temperature (red) of the current printing to cold raster (blue) away from the nozzle; Raster fusion formation after deposition from (**b**) initial surface contacting of rasters; (**c**) heat dissipation from the current deposition and neck growth; (**d**) molecular chain diffusion between rasters; (**e**) chain randomization and cold rasters.

In contrast, the low printing temperature cannot reduce the viscosity of the polymer, so the polymer chains have low mobility, causing a poor inter-raster-bonding [40]. However, the highest temperature achievable without causing degradation is not always the best printing temperature. Tian et al. [35] found that excessive temperature decreased surface accuracy when testing with continuous carbon fibre reinforced PLA. Moreover, heating the material to the completely melted state while printing could induce pores in the inner structure of the printed part, which reduces the strength [39]. From a manufacturing perspective, a high nozzle temperature causes edge warping of the part, as seen in the study reported by Nazan et al. [30]. According to their findings, the optimum temperature should be high enough to allow the molten material to flow and fuse, but not too high to completely melt the polymer.

The bar chart in Figure 4 shows the range of the temperature used by several papers to achieve a proper printed part with different types of polymers. It can be seen that the low-end polymers (low mechanical performance thermoplastic e.g., ABS, PLA, etc.) can

be fabricated at lower processing temperature than the high-end polymers (PEI, PEEK). The amorphous thermoplastics, such as ABS or PP, have a wide processing temperature range because of the difference in the crystallinity structure. Comparing the neat polymers to fibre reinforced samples, the short fibre reinforced plastics and the neat polymers can be printed using similar nozzle temperature. Yet, for continuous fibre reinforced plastics, different level of temperature is used, e.g., PLA reinforced with continuous fibre is printed at a higher temperature than neat PLA, while commercial continuous fibre reinforced plastic produced by Markforged are printed at a lower nozzle temperature than neat nylon.

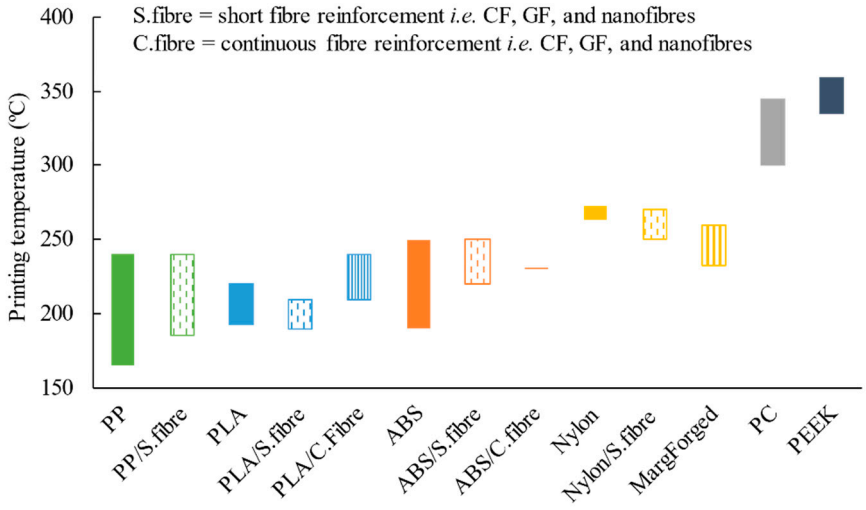

Figure 4. Printing temperature ranges using for different polymers and composite materials (the information gathered from several studies shown in Tables A1–A3).

2.4. Bed Temperature and Environmental Control

FDM can operate at room temperature and "standard" environmental conditions but environmental control can improve the performance of the printed part. The heated bed is one of the main environmental control methods. The temperature of the heater plate attached to the printing bed is usually set below the glass transition temperature of the printed filament. This heat prevents rapid cooling of the thermoplastic and improves inter-raster bonding [5]. Improper temperature control and rapid cooling can reduce the crystallinity of printed thermoplastic. General thermoplastics have low nucleation and crystallinity rates, so they cannot form a crystalline structure in a short time, this can reduce the part strength when printing without heated bed [12,43]. The heated bed could reduce the voids between rasters by improving raster fusion [18]. It has been observed that, because of the short distance from the heated bed, the raster fusion at the bottom layers is better than the higher layers [4]. The correct bed temperature also enhances the adhesion on the platform and the edge warpage can be eliminated. The environmental control can also be achieved by encasing the printer in a closed envelop that stabilizes the overall temperature and minimizes any disturbance. The trend of the selected bed temperature for neat thermoplastic filament (in Figure 5) is similar to the nozzle temperature as low-performance polymers need low bed temperature. There is no specific study for the heated bed temperature in the fibre reinforced plastic 3D printing process. However, the bed temperature of composite 3D printing was adopted from the neat polymer bed temperature with some increment as can be seen in the pre-defined bed temperature of PLA and ABS with short fibre reinforcement in Figure 5.

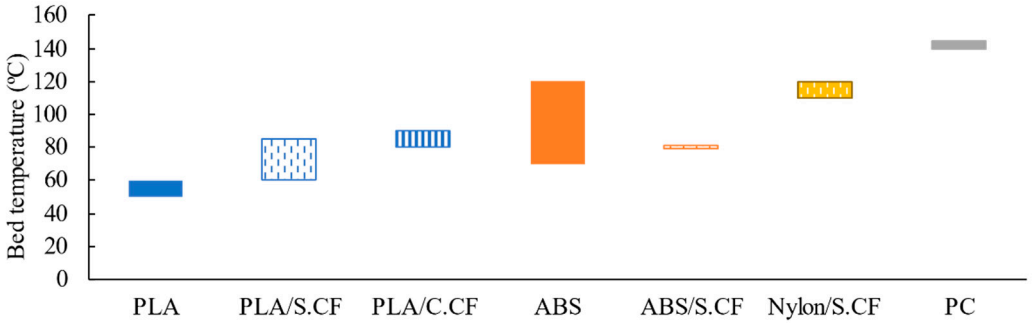

Figure 5. Bed temperature ranges using for different polymers and composite materials (the information gathered from several studies shown in Tables A1–A3).

2.5. Building Orientation

In this paper, building orientation, referring to part building principle, is categorized into three types: (a) "flat", (b) "on-edge", and (c) "upright". Figure 6 shows the different building orientations [45]. Considering dumbbell-shape 3D printed tensile testing specimen geometry, the "flat" and "on-edge" orientation deposit rasters mainly in tensile load direction (X); the "flat" (Figure 6a) builds a larger surface on the XY plane while the "on-edge" (Figure 6b) builds a smaller edge on the XY plane. By contrast, the "upright" orientation stacks layers in the Z direction (Figure 6c), so the tensile load might be applied to the Z direction accordingly to the figure axes. It can be implied that tensile strength of the "flat" and "on-edge" sample depends mainly on the strength of the material, but in the "upright" depends on the inter-raster bonding strength which is controlled by fusion between the adjacent rasters [40]. Thus, the "upright" building parts are always weaker than the others [24,28,43,45,46], the inter-raster bonding strength is always lower than the material strength.

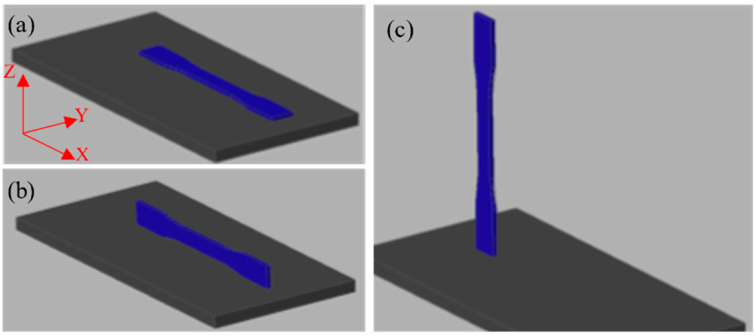

Figure 6. Building orientation definition (**a**) "flat"; (**b**) "on-edge"; (**c**) "upright". Reproduced from Smith et al. [45] with permission from Elsevier.

Comparing "flat" and "on-edge" samples of neat polymer printing, both have similar strength as a result of the same number of longitudinal rasters [46]. The difference in the strength of "on-edge" and "flat" samples have been investigated in a number of research studies. Durgan and Ertan [46] found that the "on-edge" ABS samples showed higher strength than the "flat" samples. This may be because the number of outer rasters (contour), which needs to print to be an outer shell of the 3D printed part, of "on-edge" is greater than the "flat". Another reason is that "on-edge" prints more contours in the Z direction that offers better compaction by pressure for nozzle and weight of the deposition in Z direction compared to a few layers built in the Z direction of the "flat" printing. For shear sample ([±45°] raster angle) of neat ABS and PC, in the internal structure of the "on-edge" there is a smaller contact area between crisscrossing rasters, than in the "flat", leading to a weaker through-thickness bonding of layers [24].

Considering short fibre reinforcement, the fibre reduces the flexibility of the matrix, so the softened/melted material has a high surface tension that holds the melted rasters in a circular shape. This reduces the contact area between rasters, creates inter-raster voids, and decrease interlayer strength. This leads to lower tensile strength in the "upright" direction of the short fibre reinforced sample compared to the "up-right" orientation of neat polymers [47–49]. The weakness of "up-right" orientation of chopped CF/PLA was compared to the "flat" by Ding et al. [50]. The tensile strength of the "flat" and "up-right" orientation in the article is approximately 52 MPa and 35 MPa, respectively. Wang et al. [51] compared flexural properties of the "flat" and "on-edge" printing with ABS reinforced with different short fibre types; CF, GF, KF. The author claimed that the "on-edge" shows higher energy absorption than the "flat" referring to higher flexural strength and stiffness than the "flat" specimen by 19% and 24%, respectively [51]. According to the printing of [0°/90°] raster angle with "flat" and "on-edge" in Figure 7a,b, the rasters in "on-edge" printing act as short columns resisting the bending load rather than the long beam raster in the "flat". This may be implied to the higher bending load bearing.

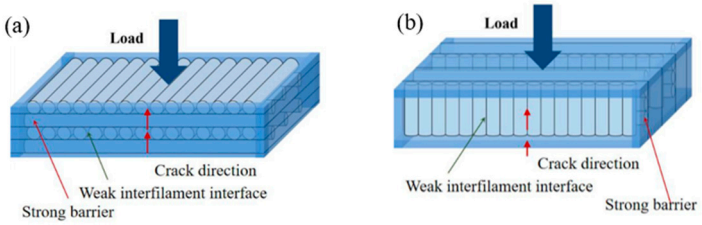

Figure 7. Different printing orientation: (**a**) "flat"; (**b**) "on-edge", printing with [0°/90°] raster angle under bending load. Reproduced from Wang et al. [51] with permission from MDPI AG.

For Markforged nylon reinforced continuous fibre, Chacón et al. [52] claimed that the "flat" building orientation shows higher fibre volume fraction than the "on-edge" by the printing principle designed by Markforged, so the "flat" has higher strength than the "on-edge". There is a comparison of impact resistance between "flat" and "on-edge" orientation of Markforged continuous fibres using Charpy impact tests. The notch was manufactured by the print path of Markforged printer. The "on-edge" shows higher impact strength than the "flat" in any types of fibre: CF, GF, KF. This relates to a difference of fibre volume content when printing with "flat" and "on-edge" orientation using Markforged printing scheme that requires neat polymer in the first and last layer. Hence, the "on-edge" orientation builds more fibre layers, in the Z direction, compared to the "flat" that deposits fibre in XY plane [53]. Figure 8 shows the tensile strength of different building orientations, raster angle, and material of each orientation are divided by filling pattern and colour (blue for PC, orange for ABS, and yellow for short fibre reinforced ABS). Overall, the strength of "flat" and "on-edge" are the same and they are higher than the "upright".

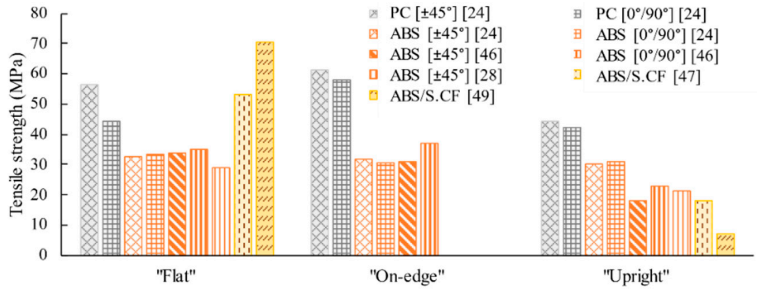

Figure 8. Tensile strength of different building orientation (the information gathered from several studies shown in Tables A1–A3). The [±45°] and [0°/90°] are the printing raster pattern described in the raster angle section (Section 2.6). The short fibre samples (ABS/S.CF) print and test mainly in the longitudinal direction.

The difference in building orientation also affects to fracture mechanic under tensile load. In neat polymer samples, the "flat" and "on-edge" have ductile behaviour (plastic dominated failure) [24]. The crack runs transversely the rasters and fail perpendicular to load direction after yielding [45,46]. By contrast, the "upright" has brittle behaviour (raster bonding dominant). Various studies observed that the crack between deposition lines or interfacial crack could leave a smooth failure surface [28,45,46]. For short jute reinforced thermoplastic printing in "upright" direction, the failure is the trans-filament fracture, due to the presence of voids [25].

The surface roughness of the different building orientation was studied in [46], printing with neat PC polymer. The "on-edge" and "upright" samples showed high surface roughness in the layer stacking direction (Z-direction) while the "flat" sample had similar surface roughness in Z and Y direction when the main printing direction along X-axis according to Figure 6a [46].

In the manufacturing process, "upright" and "on-edge" samples are more difficult to build compared to "flat" because of low attachment area to the printing bed and high stacking layers away from the heated bed that has low temperature to fuse the raster after printing [45].

2.6. Raster Angle

In this paper, raster angle is the deposition direction on an XY plane (Figure 9). The X-axis is parallel to the tensile load direction, referred to as low raster angle (0°), the Y-axis is perpendicular to the load direction, referred to as high raster angle (90°). Raster angle is a significant factor to define the strength of the printed part [4]. The building of a component usually follows two principles: a single raster angle for all layers or layer-by-layer crisscrossing raster angles.

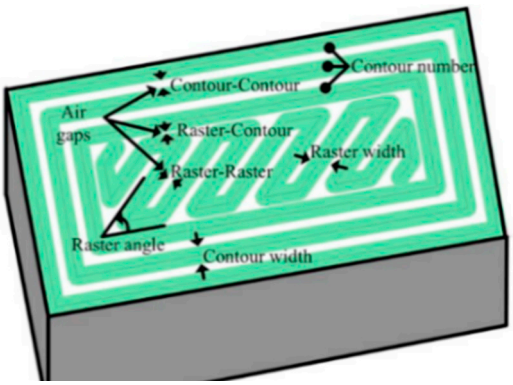

Figure 9. Description of printing parameters from top view including air gaps, raster width, number of contours, and raster width. Reproduced from Gebisa et al. [33] with permission from Elsevier.

For a single raster angle in neat polymers, the ideal angle for the tensile strength is 0°, i.e., aligned to the tensile load direction. The mechanical performance decreases when there is an increase in the raster angle as the load-bearing capabilities of the printed structure decreases [14,17,23,33,54]. For angles higher than 45°, the tensile modulus stays constant when the raster angle increases [54]. This may be caused by the fact that the component stiffness is dictated by the stiffness of the inter-raster welding, rather than the material stiffness. However, some researchers suggested different results. Song et al. [43] minimized the contour effect of PLA by cutting only the inner structure of the printed part and performed the tensile testing. They found that the 0° samples had a stress drop after yielding while the 45° had no stress drop before breakage. Onwubolu and Rayegani [26] found that the high porosity in 0° samples decreased the tensile strength, that was lower than that of 45°. Carneiro et al. [55] used a new printing procedure by printing only inner filling (infill structure described in Section 2.10) to various angles without contour, the tensile test of the new printing path shows that the 90° sample has higher mechanical

performance than 45° because of the poor fusion at the extremity of the 45° part which has no closing contour. Under tensile load, Hill and Haghi [54] found that the raster angle between 45° to 60° failed by shear of the inter-raster bonding, but the small raster angle (15° to 30°) had unpredictable failures as 15° failed at bonding following perpendicular to load failure and 30° showed interfacial failure without material failure. Figure 10 shows a generalised decrease in the tensile strength when the raster angle increases in specimens printed with a single angle. There are some cases, shown with dashed lines, which have a fluctuation in their trend.

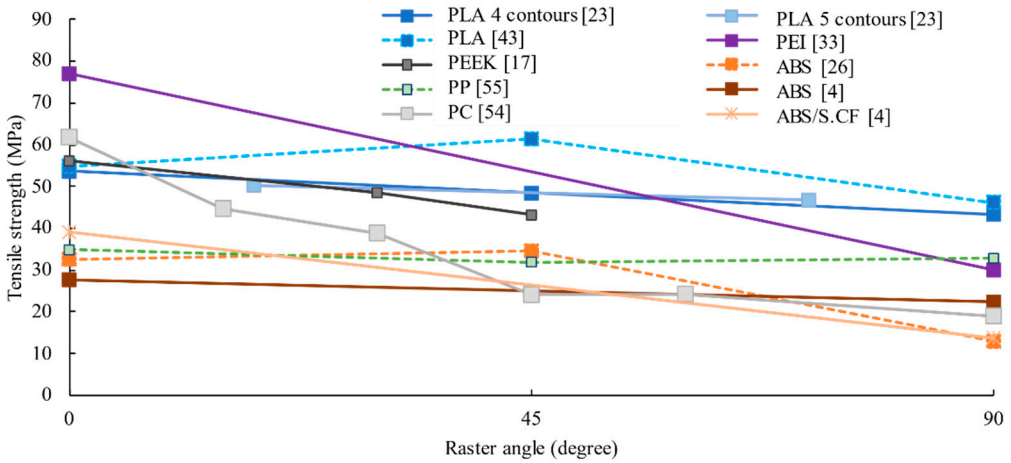

Figure 10. Tensile strength of single raster angle, normally the strength decreases as an increase in the raster angle from 0° to 90°, but there are some fluctuations shown as a dashed line that strength increases when the raster angle increases (the information gathered from several studies shown in Tables A1–A3).

In the flexural test, parts printed with a raster angle of 0° have higher bending strength and stiffness than printed with 45° or 90°, as found in Durgun and Ertan [46] study, so the low printing angle increases the flexural strength of the part. Under bending load, the 0° fails by material failure and the crack grows transverse to load direction while the 90° also fails mainly by delamination or interfacial failure according to the low bonding strength [4,54].

Considering crisscrossing raster in neat polymers, the crisscrossing is commonly used in commercial G-code generators because of their ability to distribute the stress. The balanced [±45°] is expected to be the strongest angle because of an even load distribution and the [0°/90°] crisscrossing is expected to be the weakest angle because of the loss of all material strength along the 90° angle which inter-raster-bonding dominates the tensile strength [56]. The [±45°] angle shows more uniform strain thanks to the balance in load distribution, but [0°/90°] angle shows a bi-modal strain which has a high strain in the individual 0° and 90° raster as mentioned by Cantrell et al. [24], this should cause the [0°/90°] to be weaker than [±45°]. Nevertheless, there are some deviation trends found by Carneiro et al. [55] and Cantrell et al. [24], the less effective raster angle was the [±45°] that showed lower performance than the [0°/90°]. In the PC sample, Hossian et al. [57] found a slight difference in strength between different raster angles, the highest ultimate strength was recorded in the [30°/60°] sample. By investigating inter-raster void, the [±45°] samples have diamond-shaped voids but the [0°/90°] have triangular voids. The triangular void has more contact area (~75%) than diamond-shaped voids, which generates a lower void content and a better interfacial strength [47,58]. Figure 11 shows the tensile strength when printing with different crisscrossing angle. Overall, a fluctuating trend can be observed, as mention above.

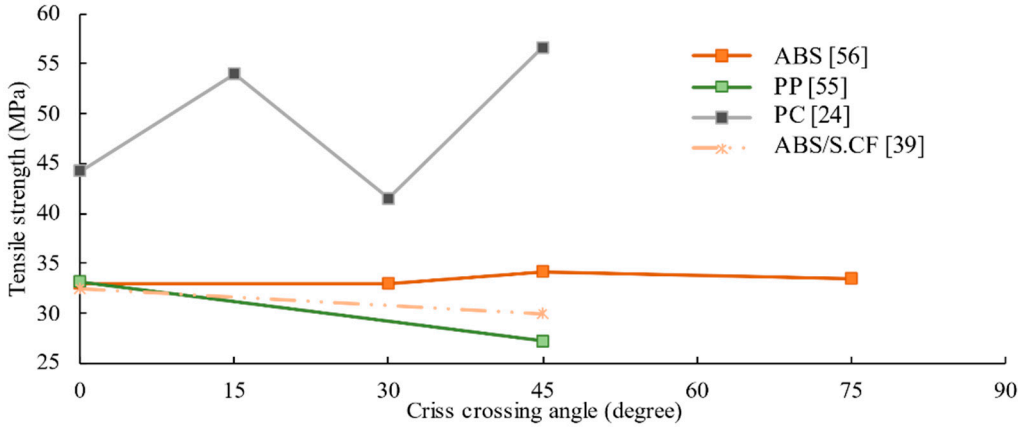

Figure 11. Tensile strength of crisscrossing raster angle of neat thermoplastic printing and composite printing (the information gathered from several studies shown in Tables A1–A3).

For fibre reinforcement samples, the fibre is supposed to be the main load-bearing component, so the alignment of the fibres in the load direction is the most efficient way to strengthen the part. Angle printing may reduce the performance of the fibre reinforcement as seen in the research conducted by Ning et al. [39] with short, approximately 0.15 mm, carbon fibre reinforcement. They found that the raster angle of [0°/90°] had better mechanical performance, i.e., higher tensile strength and stiffness, than [±45°]. Load transferring in the fibre until fibre rupture was observed in [0°/90°] samples, but fibre pull-out failure was observed in [±45°] samples. It can be inferred that the load is partially transferred to fibre, so the residual load remains in the fibre–matrix interface causing the interfacial breakage.

Zhang et al. [4] compared the difference between [±45°] crisscrossing and purely 0° or 90° printing. For neat polymer fabrication, the [±45°] raster angle has lower porosity and achieves better interface than the only one angle. With the introduction of fibre filler, the one angle printed (0° or 90°) have lower voids and show better mechanical properties than the crisscrossing.

Some studies show the relationship between the raster angle appearance and printing speed and extrusion rate using flow simulation [59,60]. The synchronized printing speed, federate and a smooth tool path (Figure 12a) can present a smoother turning radius compared to a stop-and-turn trajectory using in the conventional path (Figure 12b). This printing principle can be applied to the smaller angle printing to achieve smoother turning. In the continuous fibre printing, the Markforged continuous fibre is printed with a different aspect from the conventional printing that deposited material as a close loop from the outer to inner shown in Figure 9. The Markforged placed the fibre filament as a spiral without stopping from the outer edge to avoid cutting the continuous fibre. This refers to the smaller turning radius at the inner raster that difficult to fill with the stiff fibre showing weak spot as fibreless area and may resulting in unfinished printing as seen in Figure 12c.

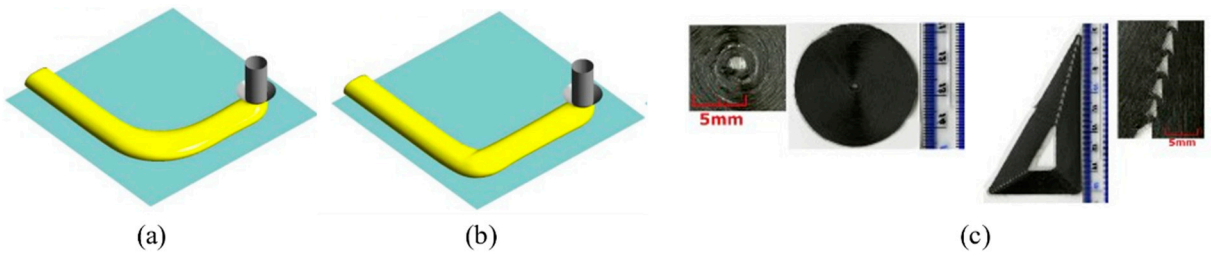

Figure 12. (**a**) Smooth radius printing path; (**b**) stop-and-turn trajectory path. Reproduced from Comminal et al. [59]; (**c**) printing of continuous fibre with the spiral printing path. Reproduced from Blok et al. [29] with permission from Elsevier.

2.7. Raster Distance (Raster Width and Air Gap)

Raster width and air gap can be adjusted by the same action. They related to the movement of the nozzle on the XY plane. The amount of material fed to the nozzle limits the raster width while the spacing between raster is called an air gap. The air gap influences part density. For "negative" air gaps, an overlap of rasters can compact them together and allows them to achieve a good interface, high part density and good flexural strength. A small gap size increases raster fusion that achieves proper polymer chain diffusion creating a good bonding interface. By contrast, for "positive" gap there is no touching between adjacent rasters being a predefined space expected for perfect raster fusion. However, an improper raster spacing leads to an imperfect bonding that causes inter-raster voids and reduces the density of the part. This results in a reduction in tensile and flexural properties. From a manufacturing perspective, the small gap consumes more material and increases the time required to finish a part compared to the larger gap, however it offers higher printing resolution. A large gap, that leaves voids, decreases part resolution and accuracy [54,56,61].

The effect of the assigned raster width on the strength was investigated by several researchers. Tian et al. [35] found that the high width created an overlap region that disrupted the printing process. Hill and Haghi [54] suggested that high width slowed down the movement of the printing head leading to longer manufacturing time and requiring more materials to build the part. Moreover, it also showed a poor surface finish. The high level of inter-raster bonding reduces the overall part strength because of the lower strength compared to the polymer strength. Thus, a large raster width, reducing the level of bonding, is beneficial to the tensile strength.

2.8. Raster Thickness

Raster thickness is defined by the distance from the nozzle outlet to the printing bed or the previous layer. The thickness is related directly to the interaction of the layers that reflects the tensile strength. Current research findings can be categorized into two groups. The first group found that a high number of interfaces reduces tensile strength. Thus, the high raster thickness decreased the number of layers minimising the interface and improving the strength. The effect is limited to only neat polymers, as shown in [14,23,55]. By contrast, another group claimed that a low raster thickness could compress layers together. Hence, achieving good compaction reduces porosity between raster and increases the interlayer bonding strength. This increases the mechanical properties, not only the tensile strength but also the flexural and shear strength. The effect can be widely seen in neat thermoplastics, short and continuous fibre reinforced thermoplastics as mentioned in [4,17,27,35,37,39,43,52]. In continuous fibre reinforcement, produced by feeding the fibres to the polymeric matrix melted pool in the nozzle (the co-extrusion method for continuous fibre reinforcement printing described in Section 3.2.1), high raster thickness produces a reduction in the fibre content by an increase in the matrix covering a fibre that leads to a decrease in strength [37]. Figure 13 shows the relationship between tensile strength and raster thickness (the solid line represents neat polymer, and the dash-dot line is the short fibre reinforced thermoplastic). There are both upwards and downwards trends; however, the average trend is a decrease in tensile strength when the thickness increases.

From a manufacturing point of view, a high thickness produces a better temperature gradient which reduces the part distortion [14,23] whilst low thickness can cause edge warping [30]. The high thickness exhibited a rough "staircase-like" pattern surface because of the imperfect fusion, this decreases overall finished sample accuracy [17,62]. The raster thickness relates to manufacturing efficiency, setting low thickness uses more material and time, increasing the cost of products. Normally, the first layer thickness is defined to be slightly lower than the other layers, in order to apply high compaction force and ensure good bed adhesion.

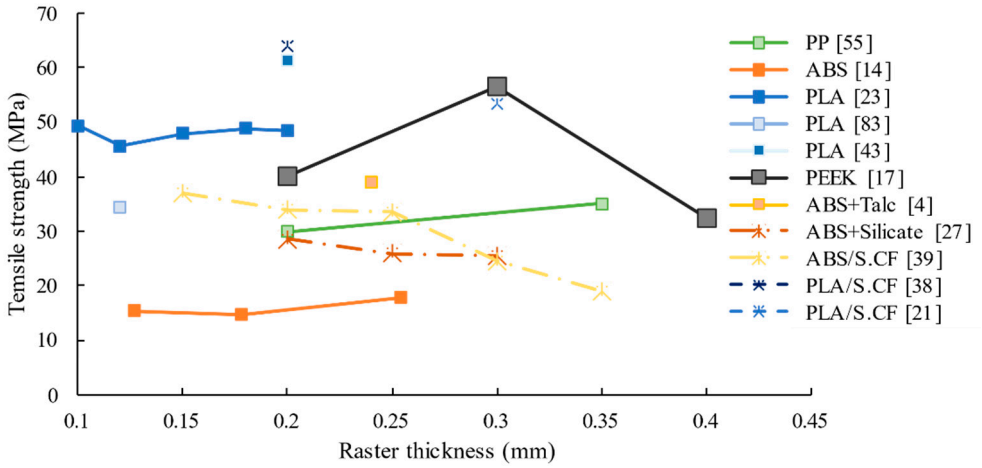

Figure 13. Tensile strength at the various thickness of neat thermoplastics and short fibre reinforced thermoplastics; most of the findings show a reduction in strength when the thickness increases (the information gathered from several studies shown in Appendix A Tables A1–A3).

2.9. Contours Numbers

By default, commercial FDM machines always generate outer shells (Figure 9) to ensure good surface finishing and reduce stress concentration at the end of the raster. The contour always runs concentrically around the part, so part of the contour always lies in the load direction despite any pre-defined (inner structure) raster angle. It can be implied that the number of contours affects tensile properties. A high number of contours increases the material laid in the load direction, increasing the tensile strength and stiffness but decreasing the elongation of the raster [8,23,33]. The number of contour lines (NC) can be defined as the product of two times the number of longitudinal raster per layer ($2n_c$), to take into account both specimen edges, and the number of layers (n_l), as shown in Equation (4) [63].

$$NC = 2n_c n_l \quad (4)$$

According to this, the contour has a high influence on the tensile properties compared to other printing parameters, e.g., printing orientation ("flat" and "on-edge") or small different raster angle. Samples with the same number of contours, but different orientations or raster angles show similar tensile properties.

2.10. Infill Volume (%Infill)

This parameter refers to the amount of material used to fill space inside the contours. The infill material is deposed within the outer contour accordingly to various patterns, e.g., rectangular, triangle, honeycomb, zigzag, or line with several raster angles, described in Section 2.6. The G-code generator can adjust the volume content of the infill from 20–100% (solid part) to change the amount of material used in the inner structure. The high %infill increases the amount of material in the part and consequently its density. Carneiro et al. [55] suggested that denser parts always have high tensile strength and stiffness because a high amount of material available to carry the load. De toro et al. [64] confirmed the state by printing nylon reinforced with 20 wt% S.CF with 100% and 60% infill and testing their properties. The 100% infill shows approximately 3 times improvement in the tensile strength and stiffness from 60%. Yasa and Ersoy [65] investigated that the change of infill percentage from 50% to 75% of the commercial Markforged chopped fibre (Onyx) increases the tensile stiffness about 6%. They continued to study on the infill percentage on toughness and found that the increase in infill from 75% to 100% resulted in a two-fold toughness improvement, but the improvement is insignificant when the shift from 50% to 70% infill [66]. However, the high amount of infill requires a high amount of material and time to complete the part, causing high manufacturing cost [23,67]. In contrast, low %infill

benefits the part accuracy. Nazan et al. [30] found that at low %infill, the rasters showed better heat diffusion than the high-density part, reducing the warping of the part.

2.11. Nozzle Geometry

Typically, the nozzle tip diameter for commercial neat thermoplastic 3D printing filament (1.5–2.85 mm in diameter) is 0.4 mm. The available diameters range from 0.1 to 0.5 mm depending on the accuracy required to the printed part and material viscosity. The continuous fibre reinforced nylon filament by Markforged, 0.35 mm filament diameter, is printed by a 0.9 mm nozzle diameter with a filleted outlet edge. The edge fillet is expected to guide the continuous fibre and promote their placement on the bed. The difference between neat thermoplastic and continuous fibre reinforced thermoplastic filament produced by Markforged is shown in Figure 14.

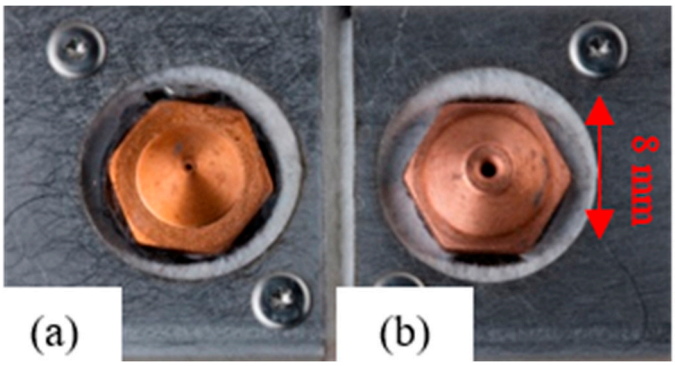

Figure 14. Markforged produced 3D printing nozzle for (**a**) neat thermoplastic 0.35 mm diameter nozzle; (**b**) nylon continuous fibre 0.9 mm diameter nozzle [68].

For normal convergent nozzle with three stages (Figure 15a), the pressure drop depends on the dimension of the large inlet section, of the conical section, and of the small outlet section. A test of feeding PLA filament through a convergent nozzle by Sukindar et al. [69] detected a large pressure drop at the small outlet diameter that causes a poor surface finish of the printed part. Yet, the high pressure drop offered a consistent material flow that increased the accuracy of the printing. The printed geometric error, calculated from conical angular and outlet diameters (Figure 15b) using Equation (5), showed that the larger nozzle diameter created higher geometric error than the smaller nozzle diameter. The nozzle diameter also links to extrusion time or fabrication time calculated with the combination of FR, the part volume (V), and total layer thickness (ΣL) using Equation (6). According to this, the small diameter requires longer times to complete the part. Sukindar et al. [69] also claimed that the optimum nozzle diameter, providing an appropriated pressure drop to maximize accuracy and minimize geometrical error, was 0.3 mm. To ensure the consistency of the printed part, Geng et al. [16] suggested that printing with a small nozzle diameter at a high speed and feed rate could maintain the same amount of deposited materials during the printing. The effect of nozzle outlet geometry was investigated also by Papon et al. [58] using carbon nanofibre/PLA polymer. Three nozzle outlet shapes with the same cross section area of 0.1257 mm^2 were studied in this research: square, star, and circle. According to the simulation, the star-shaped nozzle was predicted to deposit a smooth velocity gradient that reduced the swelling effect and provided a rectangular deposited raster cross section. This could reduce the void formation from circular raster cross section that has small contact between rasters. Figure 16 shows the different nozzle outlet geometry in the study reported by Papon et al. [58] and the simulated shape of the deposition at the different outlet geometry. Hence, nozzle shape

and size should be considered for different materials to achieve good product properties as they cause different flow behaviour.

$$ERROR = \frac{R}{\sin\left(\frac{\beta}{2}\right)} - R \tag{5}$$

$$time_{extrusion} = \frac{V}{d \times FR \times \Sigma L} \tag{6}$$

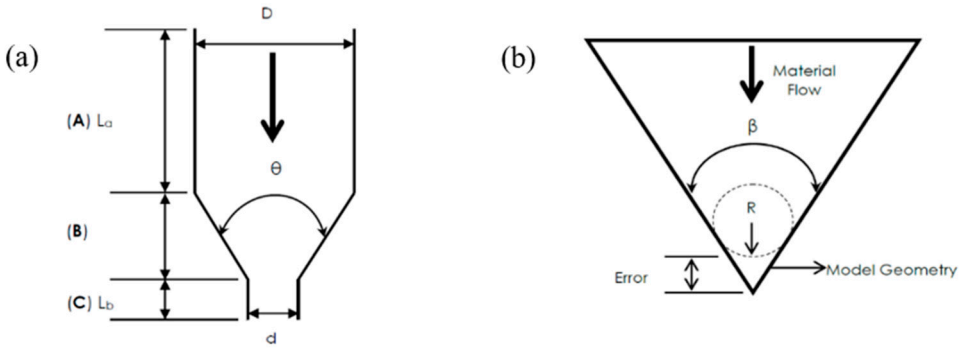

Figure 15. (**a**) Conical shape 3D printing nozzle dimension and area of pressure drop from zone A (large inlet area), B (convergence area), and C (small outlet area); (**b**) parameters for error calculation of circular nozzle, in Equation (5), where R is the radius of the extrusion orifice and β is the angle of the modelled conical nozzle geometry using in the simulation. Reproduced from Sukindar et al. [69], with permission from Jurnal Teknologi.

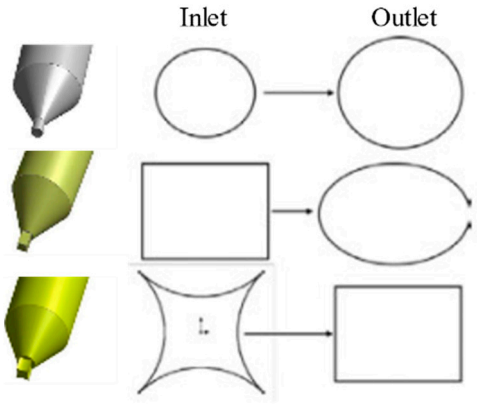

Figure 16. Investigation of the different nozzle outlet geometry: circular; square; star on the deposition geometry at the outlet using ANSYS fluent computational fluid dynamic modelling studied by Papon et al. [58].

3. Material Parameters

This section describes three types of materials used in the FDM process: thermoplastic polymers as a matrix, fibres as a reinforcement, and additional materials as a sizing agent.

3.1. Matrix

In general, the FDM process uses thermoplastic polymers that can melt at relatively low temperatures and be re-shaped in a short time. Several thermoplastics, from the low performing (e.g., PLA, ABS, and PP) to the high performing (e.g., PEEK and PEI) accordingly to their mechanical properties, as detailed in the introduction (Section 1), have been used with the FDM process. Among those materials, the most common thermoplastic used in FDM is PLA because of its low processing temperature, low shrinkage, and relatively high mechanical performance to cost ratio. Another "generic use" thermoplastic is ABS that

has better thermal conductivity than PLA, but its high viscosity hinders the fusion of the printed raster and leads to porosity in the structure [43,70]. Different classes of polyamide (e.g., PA6, PA12, PA66, etc.), also known as nylon, have a high strength compared to the first two thermoplastics, but it has poor layer adhesion and moisture absorption issues. PC is one of the best high performance among the thermoplastics, e.g., high strength, toughness, and hardness. Yet, it has high heat resistance that required high printing temperature and makes it difficult to print [71]. PEEK and PEI are the high-end thermoplastics which have high mechanical performance and require high process temperatures.

3D Matter [72] proposed a comparison of six low to medium performance thermoplastics: PLA, ABS, poly(ethylene terephthalate) (PET), nylon, thermoplastic polyurethane (TPU, rubber-like material), and PC, for FDM process, shown in Figure 17a, considering the printability, visual quality, strength, elongation at break, impact resistance, layer adhesion and heat resistance. It can be implied that the optimum thermoplastic in term of manufacturability and mechanical performance is PLA which shows relatively high mechanical performance and high printability with good visual quality, although it has a low heat resistance leading to some issues in high-temperature applications and warping on the printing bed. Another full review of the possible thermoplastics used for highly aligned discontinuous fibre thermoplastic composite FDM technology can be found in Blok et al. [70] study. This trade-off study considered several parameters, including process temperature, moulding temperature, cost, glass transition temperature, coefficient thermal expansion, thermal conductivity, shrinkage, printing ability, interfacial properties with carbon fibre, specific heat capacity, density, crystallinity, and strength. Each parameter has its weight score according to its suitability to produce composite FDM filament and then fabricate 3D printed products from the filament. Figure 17b shows that ABS is the most suitable matrix to combine with the highly aligned discontinuous fibre followed by poly(ethylene terephthalate glycol) (PETG) and PLA. This study procedure would benefit composite material developers to find a proper combination of polymer and reinforcement.

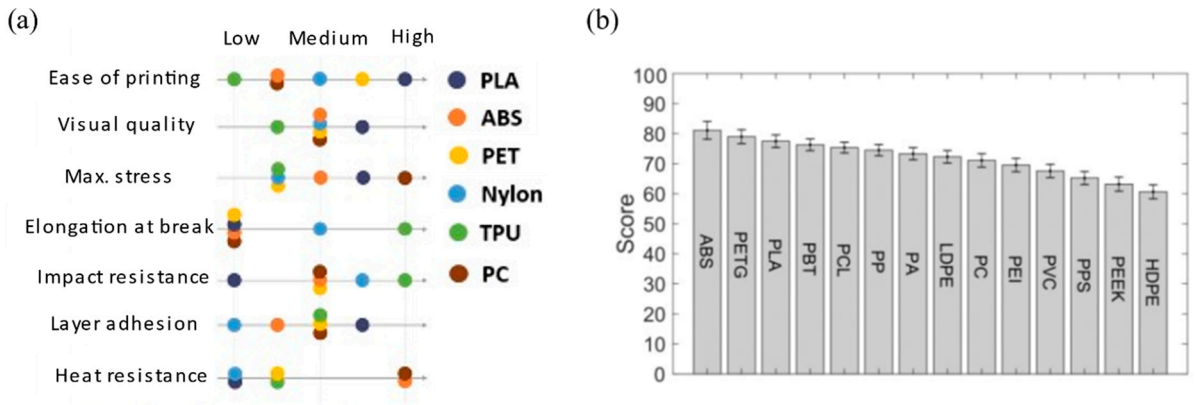

Figure 17. (**a**) Six polymers for 3D printer benchmarks according to a study from 3D Matter [72]; (**b**) sensitivity study of different thermoplastics for producing highly aligned discontinuous fibre thermoplastic 3D printing filament. Reproduced from Blok et al. [70], with permission from MDPI AG.

Focusing on the tensile strength and stiffness of polymers, the 3D printed parts (in the chequered pattern), gathered from the research papers shown Table A1, always have lower strength and stiffness than the bulk polymers filament, before printing (bulk colour), gathered from various sources in Table A4, as seen in Figure 18. This may be because of the instinct layer-by-layer manufacturing that leaves porosities, poor inter-raster bonding and rough surface finishing in the printed structure.

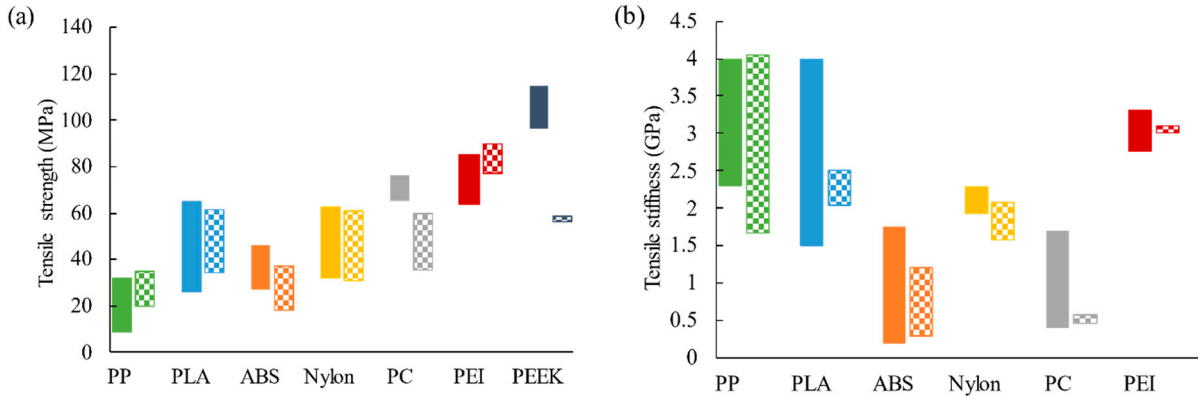

Figure 18. Range of (**a**) tensile strength; (**b**) tensile stiffness of thermoplastics as a filament (bulk) according to the information and their reference in Table A4 and as printed (checkered pattern) from Table A1.

3.2. Reinforcement

This section considers fibre reinforcement categorized accordingly to the length including nano, short, discontinuous, and continuous. Nanofibres are defined as fibre with a diameter that is less than 1 µm and an aspect ratio (the ratio between length and width) greater than 50 [73]. Critical fibre length, defined as the length that allows full load transfer from matrix to fibre, is used to classify short and discontinuous fibre. For lengths below the critical fibre length, the fibres are defined short: the load cannot be fully transferred between the fibres through the matrix, and the failure is usually fibre pull-out or matrix failure. While length above the critical length, the fibres are here defined "discontinuous" and the composite material fails for fibre breakage. The main types of fibre reinforcement; GF, CF, and KF are mainly considered in this review.

The following subsections will discuss the process to add the reinforcement to the polymeric filament and describe the effects of fibre reinforcement on the polymeric filament and the printed part. Finally, the effects of reinforcement parameters, amount of fibre and fibre length, on the part mechanical properties will be reviewed.

3.2.1. Reinforced Filament Production

Most of the research in 3D printing used commercial fibre reinforced filament produced by commercial manufacturers, e.g., Markforged, MakerBot [25] or Lulzbot TAZ [29], which have a fixed composition of each filament. Some researchers have produced their customized composite 3D printing filament so that the composition in the filament, i.e., matrix type, fibre type, fibre architecture, fibre length, the amount of fibre and sizing agents, can be changed. To produce the customized composite filament, various filament forming processes were designed. This paper divides the processes according to the fibre architecture, i.e., nano-, short, and continuous fibre mentioned above.

For nanofibre reinforcement, Shofner et al. [22] produced vapour grown carbon fibres (VGCFs) reinforced ABS by mixing both substrates with a high shear rate in a Banbury mixer. Next, the melted composite was heated and pressed to form a sheet, then the sheet was granulated. Finally, the granules were melted and extruded using a single screw extruder and spooled manually to store the 1.7 mm constant diameter filament.

For short and discontinuous fibre, the fibre is combined with the polymeric matrix using a similar method as the nanofibers: mixing and extrusion. Before the fibre–matrix mixing process, it might be necessary to chop commercial produced continuous fibre to an appropriate length for the mixing machine, typically between 1 to 3 mm, as described in [38,41,49]. The short or chopped fibres are usually blended with melted thermoplastic in a high shear rate mixing machine or twin-screw extruder at high temperature [11,31]. The melted composite could be cooled down and chopped to pellets ready to be fed to the final extrusion [11,19], or fed directly to the final extrusion, usually a single screw extruder

with a small circular die [38,49]. The final round-shaped filament diameters, range from 1.5 to 2 mm, depends on the die size. After the extrusion, the filament is cooled down at room temperature naturally or forcibly, e.g., using a cooling bath [19]. Finally, the constant cross section diameter filaments are spooled in a suitable feedstock format at temperatures around 50 °C to soften the polymer [19]. The short or discontinuous fibre reinforced matrix filament feedstock can be printed using a general FDM machine without any extra equipment. An example of a brief procedure is shown in Figure 19. Fibre breakage always occurs during the mixing and extrusion, using screw extruder, because of the high shear stress during the compound process. For example, Sang et al. [19] showed fibre breakage from the initial 1–3 mm to an average of 0.13 mm after the process. Moreover, the similar process studied by Tekinalp et al. [38] and Love et al. [49] underlined the fibre breakage from the chopped 3.2 mm to less than 0.4 mm when using Brabender Intelli-Torque Plasti-Corder prep-mixer at speed of 60 rpm for 13 min and extruding to a plunger-type batch extrusion unit to make 1.75 mm diameter filament.

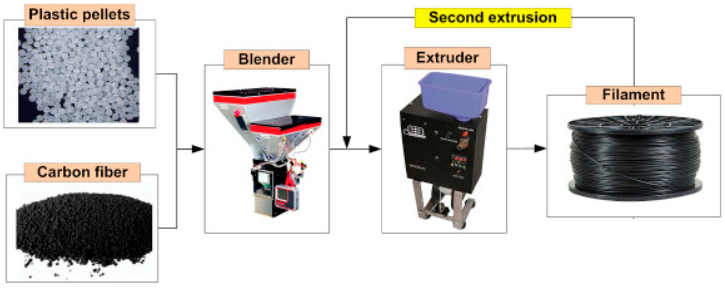

Figure 19. Short fibre FDM filament processing by mixing and extrusion. Reproduced from Ning et al. [41], with permission from Elsevier.

For continuous fibre reinforcement, there are two well-known methods to fabricate continuous fibre reinforcement. Markforged developed a pre-impregnated continuous fibre feedstock using nylon and various types of continuous fibres [29,52,74,75]. The filament is fabricated by applying tension to the fibre while passing them through a melted matrix pool. Then, the composite filament, 0.9 mm in diameter, is spooled to be stored, similarly to neat polymeric filament feedstock. This filament can be printed via normal FDM machine with some modifications: a fibre cutter to finish the fibre extrusion and a specific filleted edge nozzle as shown in Figure 14b. The fibre cutter is attached to the Markforged 3D printing machine away from the printing head to avoid adding the weight of the moving part. The second procedure to print continuous fibre is the customized method developed by many researchers [34,35,61]. The main concept of the customized continuous fibre printing is a co-extrusion method that feeds continuous dry fibre bundle to mix with the melted thermoplastic filament in the hot nozzle bath. The composite is extruded by the pressure difference between the inlet and outlet of the nozzle. The matrix used in the method is usually a normal neat thermoplastic 3D printing spool. Figure 20 shows the customized continuous 3D printer with the co-extrusion method using dry fibre and thermoplastic spool feeding to the hot nozzle and their deposition. The fibre content in the composite printing with this method depends on the fibre and matrix feed rate and printing speed e.g., feeding fibre at a higher speed than the matrix results in high fibre content, but poor fibre–matrix interface [34,35,61,76]. Obviously, the latter method, compared to the former commercial pre-impregnation, shows worse surface impregnation because of the lack of quality control after impregnation.

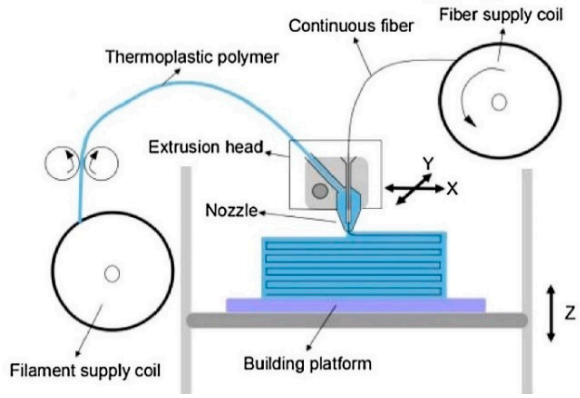

Figure 20. Customized co-extrusion, continuous FDM process feeding fibre to the melted matrix in the melted pool. Reproduced from Tian et al. [35], with permission from Elsevier.

3.2.2. Effect of Reinforcement on Microstructure

Adding fibres to the 3D printing feedstock causes the formation of voids within the filament, caused by improper fibre–matrix adhesion. Zhang et al. [4] compared the filament cross section of ABS, ABS/CNT (carbon nanotube reinforced ABS) and ABS/S.CF using scanning electron microscopy (SEM) imaging, as seen in Figure 21. It is obvious that the neat ABS filament (Figure 21a) has no inner void while voids are present in the composite material filament. According to Figure 21, ABS/S.CF filament clearly shows the largest void. The voids left in the initial filament may present as inner-raster voids in the printed part. Inner-raster voids are also found in the printed part of the Markforged continuous fibre filament because of the poor interfaces between fibre and matrix [74]. For natural fibre, the degradation temperature of the natural fibre is relatively low compared with synthetic fibres. Perez et al. [25] suggested that jute fibre degraded at the process temperature (around 180 °C). The produced gas was trapped inside the composite structure and left voids in the filament after the extrusion.

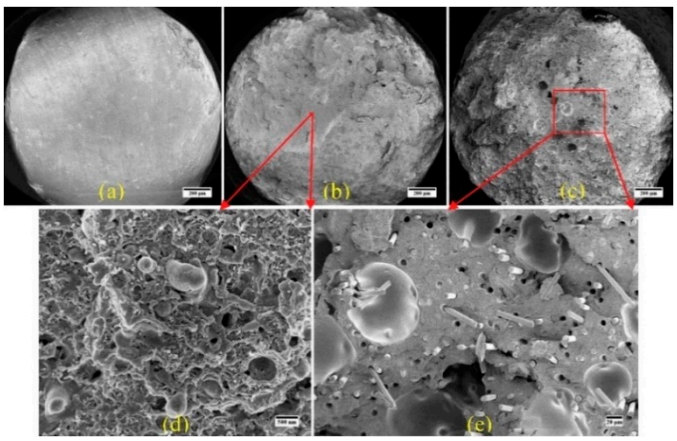

Figure 21. SEM images of the 3D printing filament with the different materials: (**a**) neat ABS; (**b**) ABS/CNT; (**c**) ABS/S.CF; (**d**,**e**) enlarging of the last two filaments. Reproduced from Zhang et al. [4], with permission from Elsevier.

3.2.3. Effect of Reinforcement on Mesostructured

Considering mesostructure of composite 3D printing parts, the fusion ability of the deposition rasters, the reinforcement increases heat diffusion of the thermoplastic and enhances the rasters fusion, causing a reduction in porosity between rasters, for example, glass fibres improved thermal properties of poly(phenylene sulphide) (PPS) [47]. This result was emphasized in a mesostructured study of ABS and ABS/S.CF by Tekinalp et al. [38]. Figure 22 shows polished cross section of ABS and ABS with different fibre content from

10–30 wt% (chopped fibre length of 3.2 mm before filament production and broken to around 0.2–0.35 mm after the mixing and extrusion depending on the fibre content). It can be seen larger triangular voids in printed neat ABS (Figure 22a) than the ABS with short CF parts Figure 22b–d. Tekinalp et al. [38] suggested that the fibres decrease die swelling phenomena, so the deposited rasters show more rectangular liked shape rather than circular shaped. The CF also increase thermal conductivity that helps raster fusion and fulfils the rectangular voids.

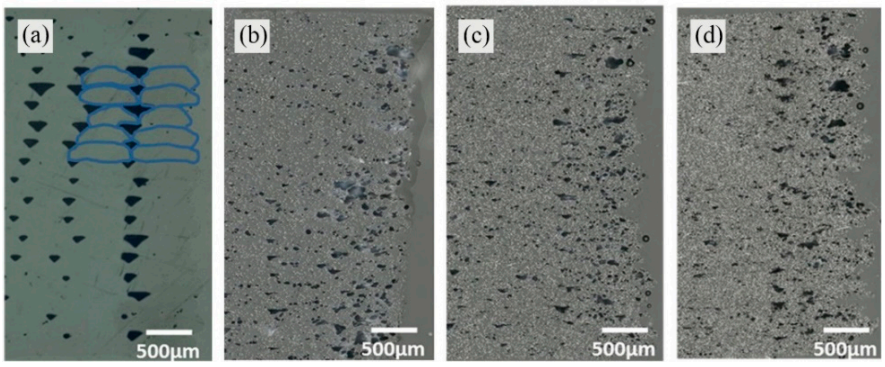

Figure 22. Micrographs of polished cross section of FDM printed part using (**a**) neat ABS; (**b**) ABS/10 wt% S.CF; (**c**) ABS/20 wt% S.CF; (**d**) ABS/30 wt% S.CF [33] with the presence of rectangular inter-raster voids. Reproduced from Tekinalp et al. [38], with permission from Elsevier.

Other articles suggested different results. Ivey et al. [12] found that the presence of the short CF in PLA (commercial filament produced by 3DXMax CFR Carbon Fiber Reinforcement PLA Filament, 3DXTech, Wyoming, MI, USA with 15 wt% of CF) increased the polymer viscosity and reduced melted flow flexibility. This hindered flowability of the melted polymeric composite to fuse to the adjacent rasters, so the depositions were imperfectly fused. It left inter-raster voids in the structure. They also commented that the high viscosity at high fibre content might cause nozzle clogging and inconsistency melted flow, so the deposition was unsteady causing large voids in structure. Duty et al. [48] mentioned that the short fibre reinforcement changed the flow field of the melted polymer and created a favourable nucleation site for bubble formation. Figure 23 shows the inter-raster voids and the ability to fuse between raster of ABS, ABS/CNT, and ABS/S.CF printed part when printing with 0° raster angle. It can be seen that the large inter-raster voids are found in the fibre reinforced thermoplastic [4]. The inter-raster void depends directly on the percentage of the fibre filler as concluded in Sang et al. [19] and Blok et al. [29].

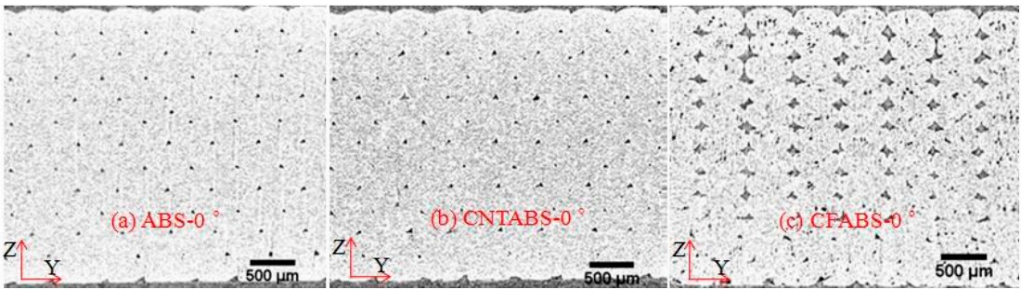

Figure 23. Cross section of printed parts from (**a**) ABS; (**b**) ABS/CNT; (**c**) ABS/S.CF with 0° raster angle and the difference in the inter-raster void formation which shows larger voids in the fibre reinforced specimen than neat ABS and nanofibre samples. Reproduced from Zhang et al. [4], with permission from Elsevier.

The effect of fibre on the mesostructure of the FDM part is ambiguous (from Figures 22 and 23). However, the latter effect, that the fibre reduces the raster fusion

leading to inter-raster voids, were more extensively published than the improvement in mesostructure when adding fibres. This may depend on several variables such as fibre–matrix compatibility or sizing agent added to composites.

3.2.4. Effect of Reinforcement on Physical and Chemical Properties

The volume of crystalline structure within polymer increases with the addition of fibre reinforcement. Sang et al. [19] stated that fibre reinforcement promoted the formation of crystalline structures from the amorphous phase by decreasing crystalline temperature. Liao et al. [31] suggested that the presence of carbon fibre in nylon reduced nucleation free energy and allowed the molecular chain to arrange into a crystallized phased because the fibre acted as an efficient nucleating agent for the crystallization.

The fibre reinforcement rises the degradation temperature of the polymer because it performs like a thermal stabilizer that absorbs heat [31]. This, however, has a very small influence on process temperatures especially T_m and T_g [19,31].

The presence of fibres improves the heat conductivity of the composite and the capabilities related directly with the fibre content [29]. The improvement in the heat conductivity helps residual heat from the previously deposited raster to transfer to the recent deposition, increasing the inter-raster bonding and part strength. The better heat transfer of fibre reinforced filament than neat thermoplastics, caused by the presence of fibres, reduces the thermal residual stress and local high temperature points, so the weak points are eliminated [29,47]. Furthermore, the presence of fibres decreases the coefficient thermal expansion (CTE), preventing warping during fabrication and improving dimension accuracy [29,77]. Owing to the random short fibre alignment in anisotropic fibre reinforced thermoplastic, the direction and amount of conductivity cannot be controlled. To achieve a controllable conductive direction of short fibre composite, the fibre alignment technology was introduced [78].

Different fibre architectures show different effects on polymeric matrix viscosity. A kind of nanofibres, VGCFs, have an insignificant effect on the viscosity, as suggested by Shofner et al. [22]. Sang et al. [19] claimed that short fibres increased the complex viscosity of the molten matrix proportionally to their content. Ivey et al. [12] suggested that a large amount of short fibre reinforcement in the matrix might result in nozzle clogging, caused not only by the fibre entanglement but also by the lack of backpressure to push the melted filament through the nozzle. Considering short fibre reinforcement, the viscosity of PLA/S.CF is higher than short basalt fibre (BF), so the PLA/S.BF has high printability than carbon fibre [19]. Moreover, Zhang et al. [4] claimed that short carbon fibre restricted flow during printing, thus the raster fusion was diminished, resulting in inter-raster voids.

3.2.5. Effect of Reinforcement on Mechanical Properties

Overall, the reinforcements aim to improve the mechanical performance of thermoplastics. Shofner et al. [22] investigated the effect of a nanofibre, VGCFs, on ABS static tensile test, accordingly to ASTM D638, and dynamic properties, following a DMTA procedure. The findings indicated that the VGCFs increased tensile properties, 40% in tensile strength and 60% in tensile stiffness, and storage modulus of ABS. Gardner et al. [10] found that CNT yarn improved the strength of PEI, but it had less effect on the stiffness and strain to failure.

For short fibre, commercial short GF reinforced PP filament, e.g., Niroumand Polymer Company (Iran) used by Sodeifian et al. [15] and SOFTER used by Carneiro et al. [55], shows an improvement in strength and stiffness form neat PP. Short CF increases the mechanical performance of thermoplastic, especially in the load direction. The stiffness of the CF composite 3D printed parts clearly improves, as confirmed by many articles [12,21,41,47], for example, 400% improvement from neat ABS when adding 13 wt% of CF with 3.2 mm long chopped fibre (before mixing and it is expected to be broken during the filament production) claimed by Love et al. [49]. The strength of the CF composite parts also increases, but less significantly than the stiffness [13,41]. This might be because of the plastic dominated

failure. As detailed in Ferreira et al. [21], PLA carried most of the stress in PLA/S.CF composite (estimated fibre length of 60 µm after filament production and printing) at the failure instead of the fibre reinforcement. The presence of fibre changes the material behaviour from ductile to more brittle with a reduction in the failure strain [12,21]. By contrast, in the through-thickness direction, the presence of short CF fibre, in Love et al. [49] study mentioned above, diminishes through-thickness tensile strength. This is mainly because the through-thickness mechanical properties depend on the raster bonding strength and the fibre restricts interlayer bonding as mentioned above.

For continuous fibre reinforcement, the mechanical performance of the composite substantially increases due to the continuous nature of the fibre that can transfer load along the length. A good example is Matsuzaki et al. [76] who reported a continuous CF-PLA co-extrusion 3D printed composite that showed a 600% improvement in tensile strength. Brenken et al. [40] claimed that the mechanical improvement of the continuous fibre reinforced thermoplastic materials had mechanical performance comparable to those of aluminium grade material. The study of Zhou et al. [74] in flexural properties of the continuous fibre reinforcement produced by Markforged also showed an 11-fold improvement in flexural strength from neat nylon printed with the same procedure (395 MPa of continuous fibre compared to 32 MPa for neat nylon). Some articles [61,75] applied the rule of mixture to describe the mechanical behaviour of continuous fibre printed materials. They mentioned that the mechanical properties of composite materials printed by FDM technology did not comply with the rule, being always lower than the ones theoretically predicted. This is because of poor fibre–matrix interface and porosity in the structure instinct in the layer-by-layer technology. Comparing the different types of continuous fibre including CF, GF, and KF produced by Markforged, CF shows the higher mechanical properties in the tensile and flexural tests [52]. Although the continuous fibre composite material has high mechanical performance, the continuum of stiff fibre causes low flexibility, this may result in manufacturing defects, i.e., fibre waviness. In the layer-by-layer deposition: the low flexibility fibre cannot fill a small radius leading to the fibreless area seen in Figure 24a, compared to nylon/S.CF printed sample as a square shape produced by Lulzbot TAZ 6 printer (Figure 24b). The manufacturing defects, being weak areas, reduce the full performance of continuous fibre [52].

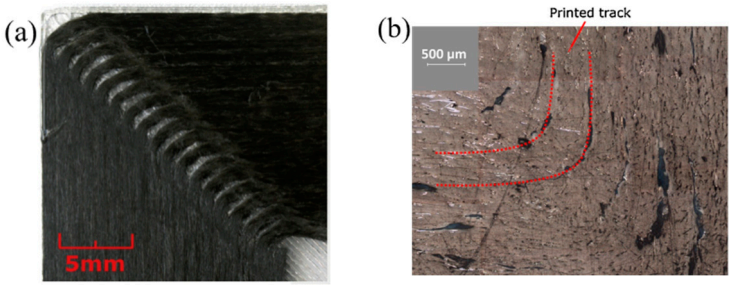

Figure 24. (**a**) Fibreless area inspected in continuous fibre printed parts; (**b**) small space between raster of short fibre printed part. Reproduced from Blok et al. [29], with permission from Elsevier.

Figure 25 shows the improvement of tensile strength in longitudinal fibre direction in different fibre reinforcement formations from neat polymers, nano-, short to continuous fibre in ABS, PLA, and nylon. The nanofibre reinforcement strength is similar to that of the neat polymers. Short fibre reinforcement shows a moderate improvement with an obvious higher strength than the neat polymers. The continuous fibre reinforcement shows a substantial increase in the tensile strength and the best reinforcement is the commercial continuous CF-nylon produced by Markforged which is ten times stronger than neat nylon. Others customized continuous fibre reinforcement produced by some researchers using ABS and PLA show an increase between 2- and 3-fold in tensile strength because of the poor interface and fibre wetting.

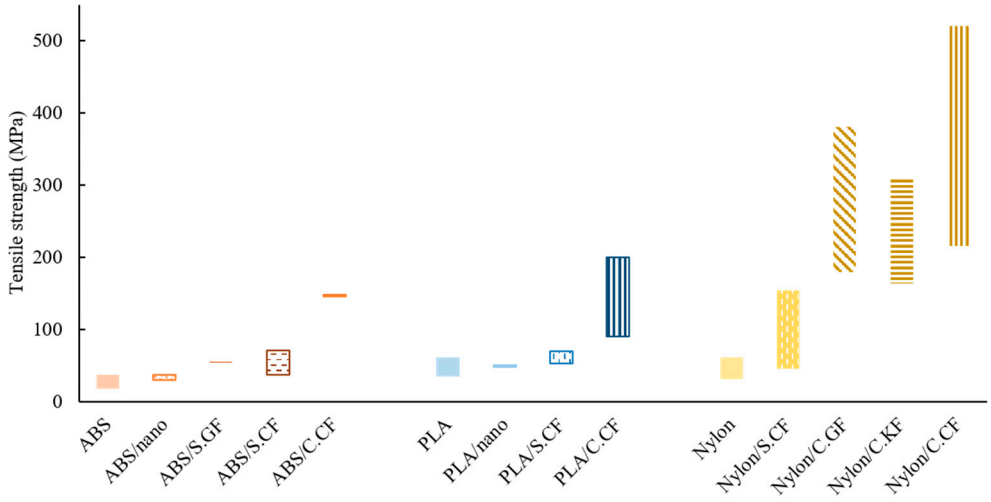

Figure 25. Tensile strength of several reinforcement types: carbon fibre (CF), glass fibre (GF), and *para*-aramid fibre (Kevlar fibre, KF), and architectures: nano-, short, and continuous, with ABS, PLA, and nylon (the information was gathered from several studies shown in Tables A1–A3).

3.2.6. Effect of Reinforcement on Failure Mechanisms

Fibre reinforcement changes the failure mechanism of the thermoplastic filament from ductile to brittle and causes the printed components to fail under various reasons. Most of the nano and short fibre reinforcement composites show pull-out failure because of the fibre length is below the critical length, and the load cannot fully transfer to fibres, and because of the poor fibre–matrix interface [13,22,28]. The effect of poor adhesion was emphasised by Hofstätter et al. [79]. They observed that the imperfectly round cross section of fibre created gaps that were difficult to be filled by viscous matrix, leading to the poor interface. In this study, 40% of the fibres in load direction were confirmed to have undergone pull-out. Liao et al. [31] observed that short fibres (15–20 mm before feedstock mixing and filament extrusion) act as a crack stopper, impeding the crack growth that meets the fibres perpendicularly, even if intuitively that could have been considered a crack nucleation point being foreign objects in neat polymers.

In continuous fibre, the tensile load parallel to the fibre direction is fully transferred amongst fibres, until failure occurs, so the expected failure of continuous fibre is fibre breakage. However, other failure modes were detected in 3D printed continuous fibre especially for those manufactured with the customized co-extrusion printing method (described in Section 3.2.1). A mixed-mode failure of fibre breakage and fibre pull-out, due to imperfect wetting in the nozzle and poor interfacial bonding, occurred in various continuous fibre specimens [5,34,61,76].

Even though the impregnation of fibre–matrix in commercial 3D printing continuous fibre Markforged filament is expected to be better than the customized co-extrusion methods, failures of CF Markforged 3D printed part under tensile load, observed by Chacón et al. [52], were extensively fibre pull-out and minor fibre breakage due to improper coating and poor interfacial bonding. They mentioned that the thermoplastic coated the outer surface of the fibre bundle while the internal fibres were hardly infiltrated, so the fibre–matrix adhesion was relatively low compared to vacuum assisted thermosetting fibre impregnation. The research also found that a similar failure occurred in GF and KF, except that the CF specimen broke perpendicular to the load direction, but the others broke at several locations, in the centre of the specimen and close to end tabs, perpendicularly to the load direction and then the crack ran parallel to the load. Figure 26 shows fracture surfaces of the tensile testing specimen with different types of fibre reinforcement: CF, GF, and KF, from Chacón et al. [52] article. Al Abadi et al. [75] conducted a failure prediction using a finite element software, Abaqus, with Hashin's damage initiation theory observing that the initial damage in CF coupons was matrix tensile damage caused by tensile and shear stresses, while GF and KF

initially failed by the fibre tensile damage. Those failure modes were confirmed by their experiment. A poor fibre–matrix interface results in matrix failure, rather than fibre failure common in conventual composites, leading to a reduction in strength, which in turn, leads to low confidence in using thermoplastic 3D printing techniques for structural applications. The improvement of the interfacial strength in thermoplastic composites should be studied to increase the final product strength.

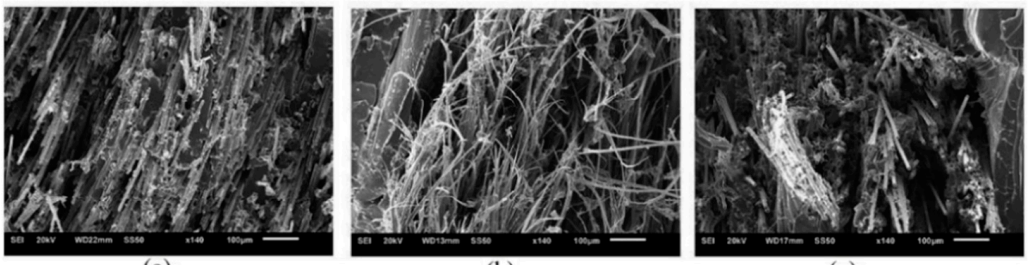

Figure 26. SEM images showing details of the fracture surface of the tensile samples with different fibres: (**a**) carbon fibre; (**b**) Kevlar fibre; (**c**) glass fibre at 140x magnification. Reproduced from Chacón et al. [52], with permission from Elsevier.

3.2.7. Effect of Fibre Length on Composite Performance

The critical fibre length is the length that determines load resistance ability. It can be calculated using Equation (7) [80] where S_c is the critical fibre length aspect ratio, σ_f is the tensile strength of fibre, τ_i is the shear strength or the shear yielding stress of the interface or the frictional shear stress at the interface, l_c is the critical fibre length and d_f is the fibre diameter.

$$S_c = \frac{\sigma_f}{2\tau_i} = \frac{l_c}{d_f} \tag{7}$$

A fibre length greater than the critical fibre length allows full load transfer causing a fibre dominated failure. In contrast, if the length is below the critical length, the applied load cannot be fully transferred through the matrix from fibres to fibre, leading to matrix failure and fibre pull-out (slippage between fibre and matrix). Normally, for the carbon fibre-epoxy case, the critical fibre length is 0.45 mm.

Ideally, the long fibre shows better mechanical performance than the short fibre [19,81]. Ning et al. [41] showed that a fibre length of 0.15 mm showed higher tensile strength and stiffness than 0.1 mm. As detailed in Section 3.2.1, the short and discontinuous fibre breakage during the filament forming process, i.e., fibre–matrix mixing and extrusion, leads to a fibre length reduction in the produced feedstock. Sang et al. [19] observed that the initial chopped 1 to 3 mm fibre can be broken down to less than 0.13 mm. The fibre length in this process has a reverse relationship with the percentage of fibre in the composite. The high percentage of fibre shows more fibre breakage that reduces the fibre length. This is because of the higher contact between fibres at the high concentration during mixing. Figure 27 shows the reduction in fibre when the fibre content increases obtaining by Tekinalp et al. [38]. This can be implied that the highest percentage of fibre cannot achieve the highest strength and the optimized fibre content of short fibre in thermoplastic composite should obtain the best mechanical properties and minimum production cost. Moreover, the fibre breakage was observed during the printing with a commercial short fibre reinforced polyamide [64]. With extremely short fibres (60 µm), Ferreira et al. [21] found a poor matrix adhesion that may result in low interfacial strength and reduce the overall part strength.

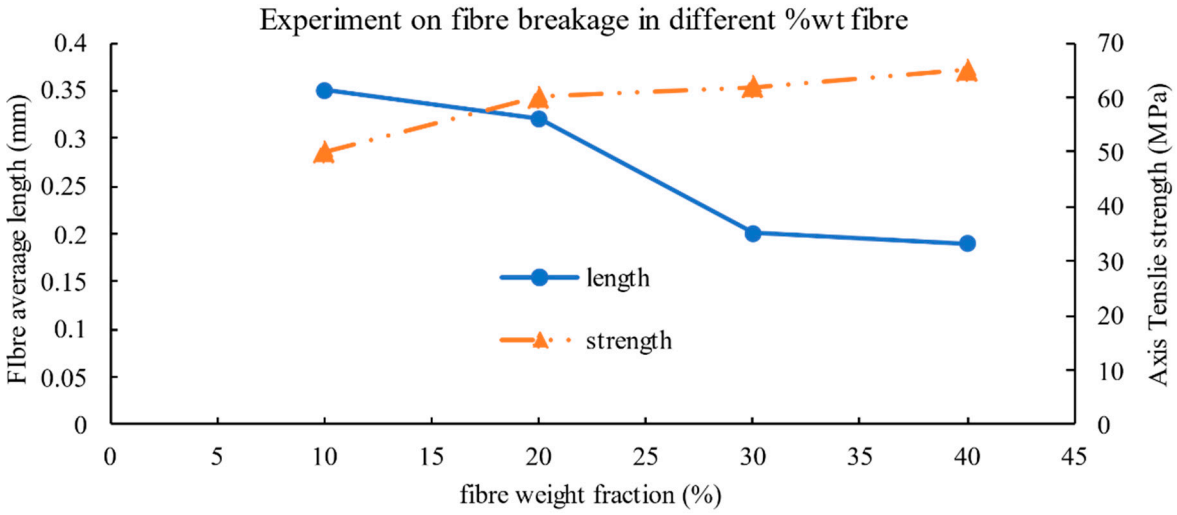

Figure 27. Fibre breakage at the high amount of fibre in the matrix resulting in minor strength improvement showing the optimized CF volume fraction to reinforce in ABS matrix suggested by Tekinalp et al. [38].

3.2.8. Effect of Fibre Content

Differences in fibre content, fibre volume fraction, or the amount of fibre filler in a composite, change the overall properties. A high fibre volume fraction is expected to be beneficial to the properties. Nevertheless, a high fraction does not always reflect into mechanical performance improvement. In the nano-reinforcement case, high content of nanofibre causes them to aggregate, reducing the printability of the filament; moreover, this has a double effect of creating a weak point in the matrix and subtracting reinforcement to the remaining material volume, reducing the part strength [13]. A high volume fraction of nanofibre increases the viscosity of the matrix causing a high surface tension of the raster, so it leads to inter-raster voids [58].

The trend described above is also found in short fibre reinforcement cases: the maximum strength and stiffness are not achieved at the highest fibre fraction. Ning et al. [41] suggested that the too high content of short CF leads to high porosity that diminished the interfacial strength. Sang et al. [19] claimed that the too high fibre content also increased viscosity, reducing the printability of the composite and causing nozzle clogging. Tekinalp et al. [38] found a nozzle clogging when adding 40 wt% of CF fibre in ABS. Figure 28a,b shows the tensile strength improvement from neat ABS and PLA when nano- and short fibres are added, and the performance loss caused by very high fibre content. The average 3D printed neat polymers strength (ABS and PLA), obtained from articles and shown in Figure 18 in the previous section, is presented as a red dash line as a baseline. In the through-thickness direction, the properties decrease with the fibre content, this is because of an increase in the viscosity that induces interlayer porosity [47].

A study by Silva et al. [18] adjusted the fibre content by selecting different fibre yarn types (1 K and 3 K) that changed the fibre volume fraction from 3.4% to 11.73%. With the customized co-extrusion printing for continuous fibre described in Section 3.2.1, the fibre content is adjusted by controlling the fibre and matrix feed rate, printing speed, raster thickness and raster width. As detailed by Tian et al. [35], the fibre content decreased with an increase in the feed rate of the polymeric filament to the melted pool, raster thickness, and raster width. This is because the same amount of fibre is covered by a higher amount of the matrix when increasing the mentioned printing parameters.

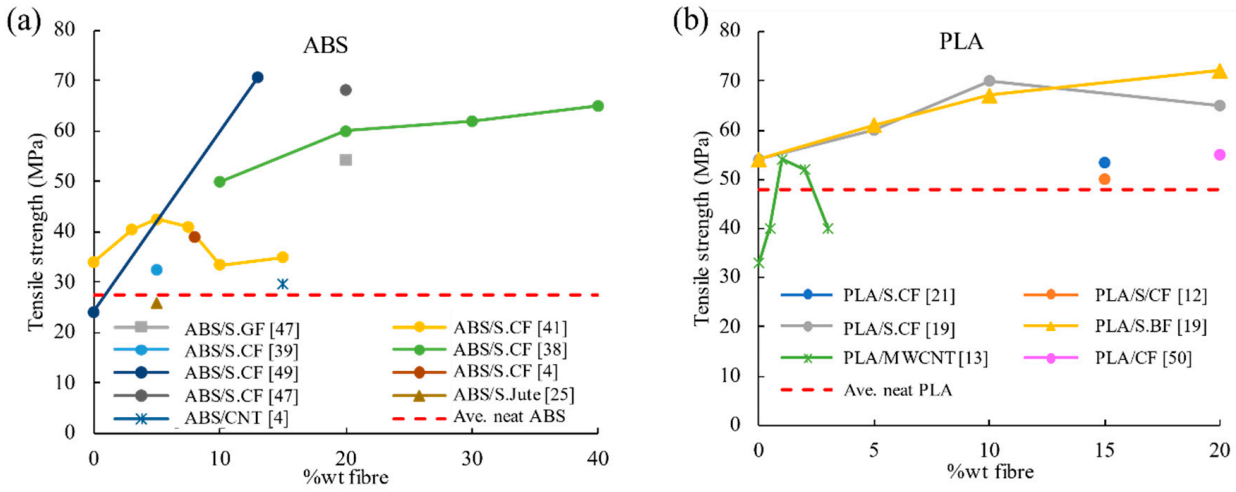

Figure 28. Tensile strength of composite FDM parts with different percentage of short fibre reinforcements in (**a**) ABS; (**b**) PLA with the average neat thermoplastics (as printed) strength shown in the red line (the information was gathered from several studies shown in Tables A1–A3).

3.2.9. Fibre Alignment during the FDM Process

The printing path can be predefined to control fibre orientation [5]. Generally, the short fibres are aligned in the nozzle moving direction with a few in the perpendicular direction [13,21,38]. This effect can be seen in both straight-line and turning radius printing paths [40]. Considering the streamline in the convergence zone of the nozzle shown in Figure 15a, a velocity gradient is generated in the flow direction, resulting in higher shear stress in the flow direction. The fibres are forced to align in the flow direction to reduce the flow resistance [31]. Hence, the fibre orientation could be estimated from the velocity and velocity gradient of the deposition using fibre orientation tensor [40,77,82]. During the printing, the re-melting of the previously deposited raster due to the next raster deposition changed the fibre orientation; the fibres were more oriented at the middle of the extrusion line and show more random orientation at the outer surface [79]. It can be inferred that the FDM process enhances fibre alignment, especially for short fibre reinforcement, along the nozzle movement direction, so the relationship of the printing path and alignment should be investigated further to improve the product performance.

3.3. Additional Materials

Additional material or sizing agents are chemical substrates added to matrix or fibre to improve the performance of composite materials. The presence of hydrated magnesium silicate (Talc, $Mg_3Si_4O_{10}(OH)_2$) in a PLA leads to an increase in melting and degradation temperature while reducing T_g [83]. In the composite material, sizing agents aim mainly to improve the interfacial strength between fibre and matrix. Linear low-density polyethylene (LLDPE) was added to ABS/GF filament to increase the ductility of the composite and hydrogenated Buna-N (an elastomer) was added to increase the compatibility of the composite to LLDPE. Plasticizers and compatibilizers in the composite could improve the strength of the part [11]. POE-g-MA was added to GF-PP composite to increase the elasticity and flexibility of the brittle composite, but an increase in POE-g-MA led to a decrease in tensile strength and more fibre pull-out failure, possibly because of degradation in the interactions between the functional groups on MA and hydroxyl group on GF [15]. BF, a poor surface interface natural fibre, was treated with a silane coupling agent (3-aminopropyl triethoxysilane) (KH550, $NH_2CH_2CH_2CH_2Si(OC_2H_5)_3$) Aladdin reagent to improve the fibre/matrix adhesion [19]. In customized co-extrusion continuous carbon fibre 3D printing, Li et al. [34] suggested a surface modification of the carbon fibre bundle to improve interfacial strength according to the process shown in Figure 29. However,

those examples of surface treatment methods and sizing agents are not always compatible with all polymers and reinforcements, so the proper additional material and method need to be investigated to achieve the best combination for specific composite materials.

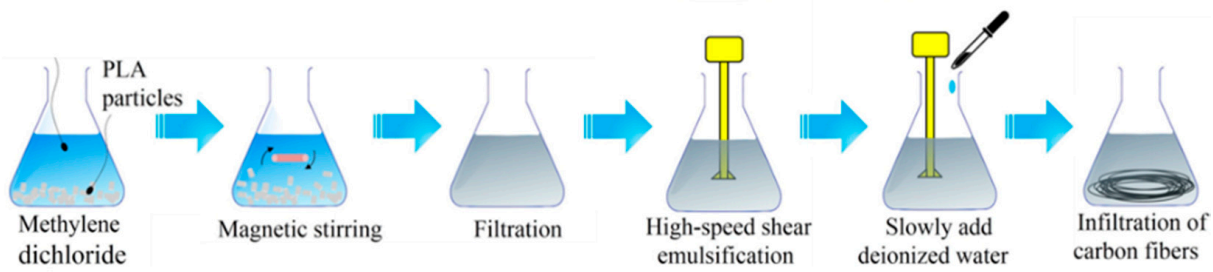

Figure 29. Surface modification of continuous carbon fibre and PLA. Reproduced from Li et al. [34], with permission from Elsevier.

4. Conclusions

In conclusion, the FDM, layer-by-layer manufacturing, allows to fabricate complex geometries within a short time, but the part quality depends significantly on the exact combination of printing parameters and the material used in the process. The printing parameters focused on this review have shown that the highest tensile strength is generally achieved by maximising the number of contours and percentage of infilled material while minimising the printing speed and the raster distance (air gap) and optimizing the nozzle and bed temperature. The material used in general FDM process is thermoplastics which have low mechanical performance compared to thermosetting or metals, so the neat thermoplastic FDM products are limited to the low performance applications. The fibre reinforcement with different architectures and fibre content is a mechanical performance improvement. Long and continuous fibre offers the highest performance improvement because of its load transferring ability. The short fibre reinforcement shows a lower mechanical performance improvement than the continuous, but it has high flexibility and formability. Although the addition of fibres improves the overall performance, it degrades the internal structure of the filament because of the poor fibre–matrix interface. Moreover, the fibre hinders the printed raster fusion, leading to poor inter-raster bonding and porous structure in the printed part. The microstructure interface can be solved by surface treatment procedures such as adding sizing, and the poor inter-raster fusion can be minimized by optimizing the printing parameters. Figure 30 proposes an overview of the process, both printing and material, parameters, that allows achieving the highest tensile strength and other properties improvement.

Among the gathered articles, using composite materials in the FDM process has shown promising initial results, but there are several research gaps in the use of fibre as a reinforcement to thermoplastic in FDM applications. Although the continuous fibre shows the best strength improvement, it creates defects, i.e., fibre-free areas and fibre waviness, because of their poor formability. To optimize the formability and mechanical properties, discontinuous fibre, which is longer than the critical fibre length, should be considered as a reinforcement. The available filament production processes may be inappropriate to produce discontinuous fibre reinforced thermoplastic filaments because the mixing and extrusion method breaks the fibres, and the discontinuous fibres cannot pultrude through thermoplastic melting bath like the continuous fibres. A new method should be developed to preserve an appropriate fibre length. Aligned discontinuous fibres represent the optimal compromised between formability, that is optimal for short fibres and poor for continuous fibres, and the mechanical performances, that are optimal for continuous fibres and poor for short fibres. Not only fibre architecture but also fibre alignment defines the mechanical performance of composite materials. Obviously, the FDM process offers better alignment than other moulding technique, but a few publications studied the printing parameters

effects on the fibre alignment of short and discontinuous fibre in thermoplastic FDM process. The possible parameters that may enhance the alignment would be printing speed and material feed rate. To realise the aligned discontinuous fibre composite material for FDM process, some works need to be done, e.g., an investigation of fibre alignment techniques before filament processing, the FDM filament forming using the aligned discontinuous fibre thermoplastic as the initial material and manufacturability of the produced filament.

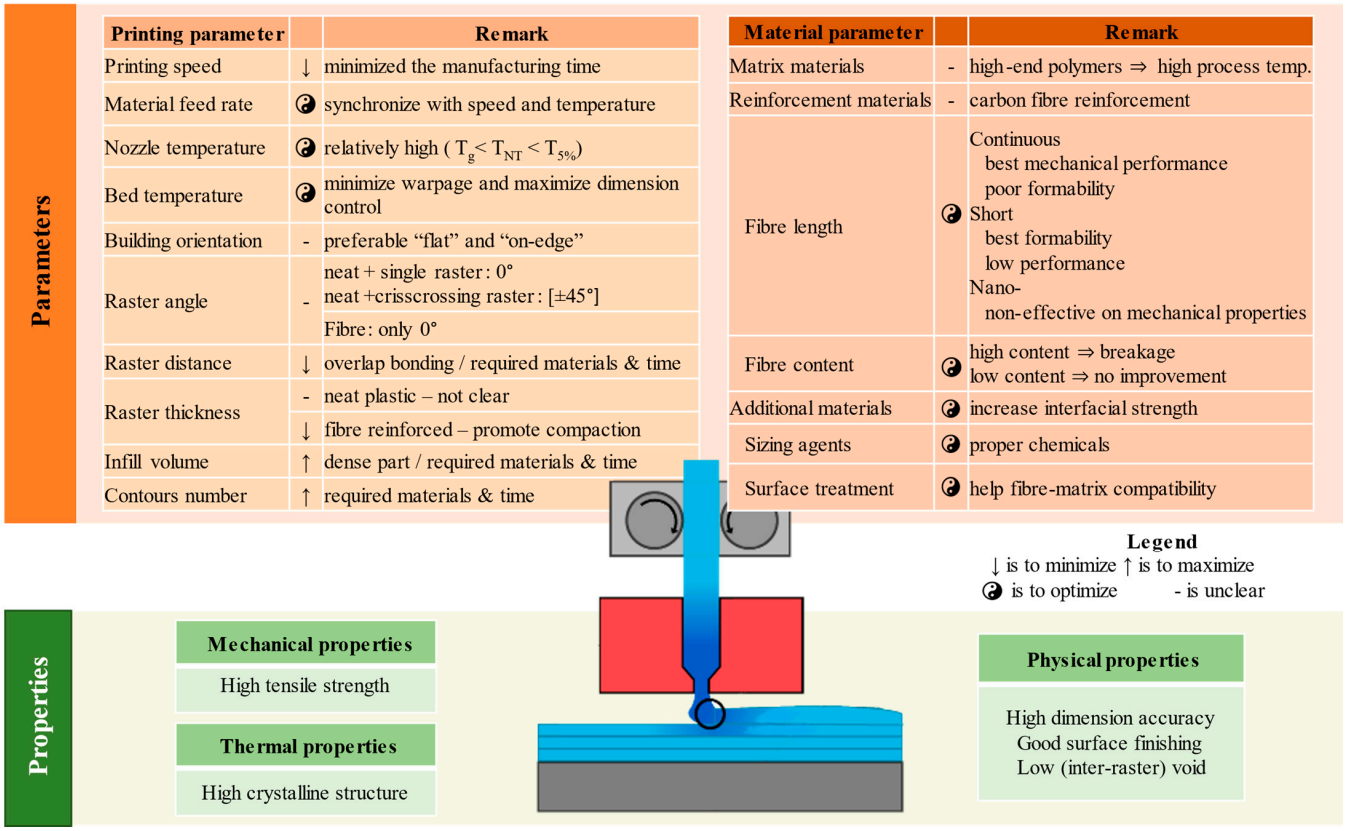

Figure 30. Printing and material parameters, that can be assigned to the FDM process to high tensile strength and the outgrowths form the setting such as crystalline structure, low porosity, and surface finishing.

Author Contributions: Conceptualization, all authors; writing—original draft preparation, N.K.; writing—review and editing, all authors; supervision, M.L.L., L.G.B., I.H., B.K.S.W. and D.S.I.; All authors have read and agreed to the published version of the manuscript.

Funding: This work was supported by the Engineering and Physical Sciences Research Council (EPSRC) through the ACCIS Doctoral Training Centre [EP/L016028/1] and the EPSRC "High Performance Discontinuous Fibre Composites a sustainable route to the next generation of composites" [EP/P027393/1] grant. N.K. is supported by the Royal Thai Government scholarship provided by the Office of the Civil Service Commission (OCSC), Royal Government of Thailand. All data required for reproducibility are provided within the paper, further supporting information can be requested from the corresponding author.

Conflicts of Interest: The authors declare no conflict of interest.

Abbreviations

%infill	Infill volume	PC	Polycarbonate
ABS	Poly(acrylonitrile-butadiene-styrene)	PEEK	Poly(ether ether ketone)
ALM	Additive layer manufacturing	PEI	Polyetherimide
BF	Basalt fibre	PET	Poly(ethylene terephthalate)

C.	Continuous fibre	PETG	Poly(ethylene terephthalate glycol)
CF	Carbon fibre	PLA	Poly(lactic acid)
CNT	Carbon nanotube	PP	Polypropylene
FDM	Fused deposition modelling	S.	Short fibre
FR	Feed rate of filament	$T_{5\%}$	Degradation temperature, 5% mass loss
GF	Glass fibre	T_D	Calculated composite density
KF	Kevlar fibre, aramid fibre	T_g	Glass transition temperature
LLDPE	Linear low-density polyethylene	T_m	Melting temperature
MWCNT	Multi-Walled Carbon Nanotubes	TPU	Thermoplastic polyurethane
NC	Number of contours	VGCFs	Vapour grown carbon fibres
PA	Polyamide, Nylon	wt%	Percentage by weight

Appendix A

The following tables gather parameters: printing and material used to produce the testing specimens and the testing results. The graphs in this paper are plotted according to this information.

Table A1. Summary of parametric study in neat thermoplastic of the FDM process.

Study	Material Parameters					Printing Parameters								Tensile Properties	
	Polymer	Reinforcement													
		Material	Length (mm)	Diameter (μm)	Content (by wt%)	Print Speed (mm/min)	Nozzle Temp. (°C)	Bed Temp. (°C)	Build Orientation F, E, Z	Raster Angle (degree)	Raster Thickness (mm)	Infill Volume (%)	Contour (Lines)	Stiffness (GPa)	Ultimate Strength (MPa)
Carneiro et al. [55]	PP					3600	165	room		45, 0, 90, [±45], [0/90]	0.2, 0.35	20, 60, 100		0.3–1.2	10–35
Sood et al. [14]	ABS								F	[0/90], [15/75], [30/60], [±45]	0.127, 0.178, 0.254				9.95–18.09
Onwubolu and Rayegani [26]	ABS								F	0, 45, 90	0.127, 0.330				4.01–34.61
Croccolo et al. [63]	ABS								F, E	±45	0.25		1, 4, 7, 10	1.81–2.11	23.9–29.7
Durgun and Ertan [46]	ABS								F, E, Z	0, 30, 45, 60, 90	0.253			1.9–2.5	19–37
Dawoud et al. [56]	ABS					1800	250	120		[0/90], [30/60], [±45], [75/15]	0.5		1		28–35
Cantrell et al. [24]	ABS						235	105	F, E, Z	[0/90], [±45]	0.1			1.96–2.05	30.0–32.8
Zhang et al. [4]	ABS					3600, 4800, 6000				0, [±45], 90	0.18, 0.24, 0.3			1.95–2.44	22.31–27.69
Walter et al. [28]	ABS								F	[±45]	0.25			1.89–2.18	21.5–28.8
Duty et al. [47]	ABS						250	95						2.3–2.41	31.2–34
Cicala et al. [83]	PLA					2100–2700	210	50		[0/90]	0.12	100		2.66–3.74	28.37–34.43
Song et al. [43]	PLA					2700, 3600, 6000, 9000	200, 210, 220, 230		E	0, 45, 90	0.1, 0.2, 0.3, 0.4			3.96–4.04	46.24–61.42
Lanzotti et al. [23]	PLA					3600	205	60	F	0, 18, 45, 72, 90	0.1, 0.12, 0.15, 0.18, 0.2	100	2, 3, 4, 5, 6	2.79–3.49	37.62–53.59
Ivey et al. [12]	PLA					1800^{1st} 2100^{rest}	200	85		[0/90]	0.1	100	2	3.37	59.3
Papon et al. [58]	PLA					1200	220	110		$[45/-45/45/90/0]_S$	0.4	100		1.670	45
Dickson et al. [84]	Nylon									concentric, 0				0.53	61
Chacón et al. [52]	Nylon						274		F, E	0	0.1, 0.125, 0.2	100		0.41–0.47	27.2–30.9
Cantrell et al. [24]	PC						345	145	F, E, Z	[0/90], [30/60], [±45], [75/15]				1.62–2	30.4–43.5
Hill and Haghi [54]	PC						300		F	0, 15, 30, 45, 60, 75, 90	0.267			1.35–2.082	16.89–59.77
Smith and Dean [45]	PC								F, E, Z	[0/90]	0.508			1.18–1.57	20.6–35.7
Hossain et al. [57]	PC						345	140		[0/90], [30/60], [±45]	0.432–0.508			1.5–1.83	45–55
Wu et al. [17]	PEEK						334		F	0, 30, 45	0.2, 0.3, 0.4		2		32.4–56.6
Gebisa and Lemu [33]	PEI								F	0, 90			1, 5		26–77
Gardner et al. [10]	PEI						375	162		0				3	90

Table A2. Summary of parametric study in nano/short fibre thermoplastic FDM process.

Study	Material Parameters					Printing Parameters								Tensile Properties	
	Polymer	Reinforcement													
		Material	Length (mm)	Diameter (μm)	Content (by wt%)	Print Speed (mm/min)	Nozzle Temp. (°C)	Bed Temp. (°C)	Build Orientation F, E, Z	Raster Angle (degree)	Raster Thickness (mm)	Infill Volume (%)	Contour (Lines)	Stiffness (GPa)	Ultimate Strength (MPa)
Carneiro et al. [55]	PP	GF			30	480	185			[±45]	0.2	100		1.9	40
Sodeifia et al. [15]	PP	GF					240	30			0.1, 0.4	100		0.25–0.4	20–32
Ning et al. [41]	ABS	CF	0.150, 0.100	7.2	3–15	1200 ^{1st} 1500 ^{rest}	230			[±45]	0.2	100		2–2.6	34–44
Ning et al. [39]	ABS	CF			5	15, 20, 25, 30, 35	200, 210, 220, 230, 240	80	F	[±45], [0/90]	0.15, 0.2, 0.25, 0.3, 0.35	100	3	0.6–1.1	18–37
Tekinalp et al. [38]	ABS	CF	<0.4		10–40		205				0.2			2–14	30–65
Love et al. [49]	ABS	CF	<0.4		13		220							1.52–8.91	7.0- 70.69
Duty et al. [48]	ABS	CF	1		20	3048	250			0, 90				2.13–11.92	10.27–66.18
Duty et al. [47]	ABS	CF	<3		13, 20		250	95						8.18–11.94	53.3–66.4
Zhang et al. [4]	ABS	CF			8	3600, 4800, 6000				0, [±45], 90	0.18, 0.24, 0.3			2.19–5.89	13.74–39.05
Zhong et al. [11]	ABS	GF					250	60	F, Z						24–58 kg *
Duty et al. [48]	ABS	GF	1		20	3048	250			0, 90				2.48–5.65	15.30–54.33
Duty et al. [47]	ABS	GF	<3		20		250	95						5.67	54.4
Perez et al. [25]	ABS	Jute			5	3300	230				0.27			0.871–1.543	12.9–25.9
Perez et al. [25]	ABS	Nano TiO_2			5	3300	230				0.27			1.355–1.708	18.4–32.2
Zhang et al. [4]	ABS	CNTCF			15	3600, 4800, 6000				0, [±45], 90	0.18, 0.24, 0.4			2.01–2.52	21.46–29.64
Shofner et al. [22]	ABS	VGCFs	0.1	0.1	10										37
Ferreira et al. [21]	PLA	CF	0.06		15	3000	190	70		0, 90	0.3	100		4.14–7.66	35.4–53.4
Sang et al. [19]	PLA	CF	0.131	7	5–20	1200 ^{1st} 3600 ^{rest}	210	60		[±45]	0.1	100		3.4–7.4	60–70
Ivey et al. [12]	PLA	CF	0.125	7.4	15	1800 ^{1st} 2100 ^{rest}	200	85		0/90	0.1	100	2	5.68	55.2
Sang et al. [19]	PLA	BF	0.13	12	5–20	1200 ^{1st} 3600 ^{rest}	210	60		[±45]	0.1	100		3–5.5	61–70
Isobe et al. [13]	PLA	MW CNT			0.5–3									~3–3.5	40–50
Papon et al. [58]	PLA	nano CF	0.0005	0.05	0.5–2	1200	220	110		$[\pm 45/45/90/0]_s$	0.4	100		1.822	41–48
Blok et al. [29]	nylon	micro CF	0.1		6		260		F		0.2			1.85	33.5
Isobe et al. [13]	nylon	CF	0.13		14.3									~1–2	45.5
Silva and Rezende [18]	nylon	CF	0.05–0.2	5	65	300	270	110			1			3.5	153.62
Liao et al. [31]	nylon	CF		6–7	2–10	1800	250	120		0		100		1–3.5	48–90
Walter et al. [28]	nylon	CF							F	[±45]	0.1			3.019	58.2
Duty et al. [47]	PPS	GF	<3 mm		40		357	95						10.82	51.2
Duty et al. [48]	PPS	GF	1		40	3048	251			0, 90				10.82	51.2
Gardner et al. [10]	PEI	CNT yarns					375	162		0				3	119

* The tensile test in the study was measured with a different procedure and it was present as force in kilograms.

Table A3. Summary of parametric study in continuous fibre thermoplastic FDM process.

Study	Material Parameters					Printing Parameters								Tensile Properties	
	Polymer	Reinforcement				Print Speed (mm/min)	Nozzle Temp. (°C)	Bed Temp. (°C)	Build Orientation F, E, Z	Raster Angle (degree)	Raster Thickness (mm)	Infill Volume (%)	Contour (Lines)	Stiffness (GPa)	Ultimate Strength (MPa)
		Material	Length (mm)	Diameter (μm)	Content (by wt%)										
Blok et al. [29]	nylon	CF			36.67	2.39 cm^3/hr	260			0	0.125	100		62.5	968
Isobe et al. [13]	nylon	CF			35.7					0				10	341
Zhuo et al. [74]	nylon	CF								0					
Chacón et al. [52]	nylon	CF		350	2.38–31.32		274 (nylon) 232 (fibre)		F, E	0	0.125			7.6–51.7	96.6–436.7
Al Abadi et al. [75]	nylon	CF			45					[±45]/0				37	360
Mohammadizadeh et al. [85]	nylon	CF					265 (nylon) 270 (fibre)			concentric, 0	0.125	50			235.5–404.3
van der Klift et al. [86]	nylon	CF			29.79-						0.125			15–35.7	128–520
Dickson et al. [84]	nylon	CF		350	13.59		263	NO		concentric, 0	0.125			7.73	216
Chacón et al. [52]	nylon	GF		300	3.95–33.67		273 (nylon) 232 (fibre)		F, E	0	0.1			3.7–19.6	113.4–381.2
Al Abadi et al. [75]	nylon	GF			47.62					[±45]/[0/90]				6.4	180
Mohammadizadeh et al. [85]	nylon	GF					266 (nylon) 270 (fibre)			concentric, 0	0.1	50			302.6–372.1
Dickson et al. [84]	nylon	GF		300	10.6–13.06		263	NO		concentric, 0	0.1			3.12–3.75	194–206
Chacón et al. [52]	nylon	KF		300	3.19–28.88		275 (nylon) 232 (fibre)		F, E	0	0.1			5.2–25.5	55.8–235.6
Al Abadi et al. [75]	nylon	KF			42.11					[±45]/[0/90]				8.7	170
Al Abadi et al. [75]	nylon	KF			42.11					[±45]/[0/90]				8.7	170
Mohammadizadeh et al. [85]	nylon	KF					267 (nylon) 270 (fibre)			concentric, 0	0.1	50			259.7–309.14
Dickson et al. [84]	nylon	KF		12	8.66–10.81		263	NO		concentric, 0	0.1			3.61–4.37	150–164
Matsuzaki et al. [76]	PLA	CF			9.3	60	210	80		0				20	200
Li et al. [34]	PLA	CF			<42.92										91
Tian et al. [35]	PLA	CF			34.93	100, 200, 300, 400, 500, 600	180, 190, 200, 210, 220, 230, 240	NO			0.3, 0.4, 0.5, 0.6, 0.7, 0.8				
Namiki et al. [61]	PLA	CF			1.45	100	210	80						5.8	90
Matsuzaki et al. [76]	PLA	Jute Fibre			7.11	60	210	80		0				5	50
Hou et al. [37]	PLA	KF			13.11	100	210	NO			0.1–0.			7.42	73.54
Tey et al. [87]	PLA	KF		400	6.54 %vol						0.8		4	3.29	104.64
Yang et al. [5]	ABS	CF			10	600	230	90			0.5			4.185	147

Appendix B

Table A4 shows plastics tensile strength and stiffness gathers from different sources.

Table A4. Plastic as a filament tensile strength and stiffness gathered from various sources.

PLA			ABS			PP		
Strength (MPa)	**Stiffness (GPa)**	**Ref.**	**Strength (MPa)**	**Stiffness (GPa)**	**Ref.**	**Strength (MPa)**	**Stiffness (GPa)**	**Ref.**
45.6	2.364	[88]	33.9	1.618	[89]	32	-	[90]
37	4	[91]	27	2.1–7.6	[91]	8.7	0.2	[92]
26.4	2.3	[93]	46	-	[94]	28–36	1.75	[95]
46.8	2.91	[96]	33	-	[97]	34	1.325	[98]
65	-	[90]	25–50	1.1–2.9	[99]			
PC			**Nylon**			**PEI**		
Strength (MPa)	**Stiffness (GPa)**	**Ref.**	**Strength (MPa)**	**Stiffness (GPa)**	**Ref.**	**Strength (MPa)**	**Stiffness (GPa)**	**Ref.**
72	-	[90]	48	-	[97]	81	-	[97]
65	-	[100]	32	0.4	[101]	85	3.2	[102]
76.4	2.13	[103]	34.4	0.579	[104]	64	2.77	[105]
57	1.94	[106]	45	1.4	[107]	85	3.3	[108]
68	2.28	[109]	48	1.7	[110]			
PEEK								
Strength (MPa)	**Stiffness (GPa)**	**Ref.**						
105	4.1	[111]						
115	4.3	[112]						
96.52	4.07	[113]						

References

1. Parandoush, P.; Lin, D. A review on additive manufacturing of polymer-fiber composites. *Compos. Struct.* **2017**, *182*, 36–53. [CrossRef]
2. Ngo, T.D.; Kashani, A.; Imbalzano, G.; Nguyen, K.T.Q.; Hui, D. Additive manufacturing (3D printing): A review of materials, methods, applications and challenges. *Compos. Part B Eng.* **2018**, *143*, 172–196. [CrossRef]
3. Frketic, J.; Dickens, T.; Ramakrishnan, S. Automated manufacturing and processing of fiber-reinforced polymer (FRP) composites: An additive review of contemporary and modern techniques for advanced materials manufacturing. *Addit. Manuf.* **2017**, *14*, 69–86. [CrossRef]
4. Zhang, W.; Cotton, C.; Sun, J.; Heider, D.; Gu, B.; Sun, B.; Chou, T.-W. Interfacial bonding strength of short carbon fiber/acrylonitrile-butadiene-styrene composites fabricated by fused deposition modeling. *Compos. Part B Eng.* **2018**, *137*, 51–59. [CrossRef]
5. Yang, C.; Tian, X.; Liu, T.; Cao, Y.; Li, D. 3D printing for continuous fiber reinforced thermoplastic composites: Mechanism and performance. *Rapid Prototyp. J.* **2017**, *23*, 209–215. [CrossRef]
6. Levy, G.N.; Schindel, R.; Kruth, J.-P. Rapid manufacturing and rapid tooling with layer manufacturing (LM) technologies, state of the art and future perspectives. *CIRP Ann.* **2003**, *52*, 589–609. [CrossRef]
7. Wang, X.; Jiang, M.; Zhou, Z.; Gou, J.; Hui, D. 3D printing of polymer matrix composites: A review and prospective. *Compos. Part B Eng.* **2017**, *110*, 442–458. [CrossRef]
8. Kumar, N.; Jain, P.K.; Tandon, P.; Pandey, P.M. The effect of process parameters on tensile behavior of 3D printed flexible parts of ethylene vinyl acetate (EVA). *J. Manuf. Process.* **2018**, *35*, 317–326. [CrossRef]
9. Bettini, P.; Alitta, G.; Sala, G.; Di Landro, L. Fused deposition technique for continuous fiber reinforced thermoplastic. *J. Mater. Eng. Perform.* **2017**, *26*, 843–848. [CrossRef]

10. Gardner, J.M.; Sauti, G.; Kim, J.-W.; Cano, R.J.; Wincheski, R.A.; Stelter, C.J.; Grimsley, B.W.; Working, D.C.; Siochi, E.J. *Additive Manufacturing of Multifunctional Components using High Density Carbon Nanotube Yarn Filaments*; NASA Langley Research Center: Hampton, VA, USA, 2016.
11. Zhong, W.; Li, F.; Zhang, Z.; Song, L.; Li, Z. Short fiber reinforced composites for fused deposition modeling. *Mater. Sci. Eng. A* **2001**, *301*, 125–130. [CrossRef]
12. Ivey, M.; Melenka, G.W.; Carey, J.P.; Ayranci, C. Characterizing short-fiber-reinforced composites produced using additive manufacturing. *Adv. Manuf. Polym. Compos. Sci.* **2017**, *3*, 81–91. [CrossRef]
13. Isobe, T.; Tanaka, T.; Nomura, T.; Yuasa, R. Comparison of strength of 3D printing objects using short fiber and continuous long fiber. *Proc. IOP Conf. Ser. Mater. Sci. Eng.* **2018**, 012042. [CrossRef]
14. Sood, A.K.; Ohdar, R.K.; Mahapatra, S.S. Parametric appraisal of mechanical property of fused deposition modelling processed parts. *Mater. Des.* **2009**, *31*, 287–295. [CrossRef]
15. Sodeifian, G.; Ghaseminejad, S.; Yousefi, A.A. Preparation of polypropylene/short glass fiber composite as Fused Deposition Modeling (FDM) filament. *Results Phys.* **2019**, *12*, 205–222. [CrossRef]
16. Geng, P.; Zhao, J.; Wu, W.; Ye, W.; Wang, Y.; Wang, S.; Zhang, S. Effects of extrusion speed and printing speed on the 3D printing stability of extruded PEEK filament. *J. Manuf. Process.* **2019**, *37*, 266–273. [CrossRef]
17. Wu, W.; Geng, P.; Li, G.; Zhao, D.; Zhang, H.; Zhao, J. Influence of layer thickness and raster angle on the mechanical properties of 3D-printed PEEK and a comparative mechanical study between PEEK and ABS. *Materials* **2015**, *8*, 5834–5846. [CrossRef]
18. Silva, J.V.; Rezende, R.A. Additive Manufacturing and its future impact in logistics. *IFAC Proc. Vol.* **2013**, *46*, 277–282. [CrossRef]
19. Sang, L.; Han, S.; Li, Z.; Yang, X.; Hou, W. Development of short basalt fiber reinforced polylactide composites and their feasible evaluation for 3D printing applications. *Compos. Part B Eng.* **2019**, *164*, 629–639. [CrossRef]
20. Magdum, Y.; Pandey, D.; Bankar, A.; Harshe, S.; Parab, V.; Kadam, M. Process parameter optimization for FDM 3D printer. *Int. Res. J. Eng. Technol. (IRJET)* **2019**, *6*, 1–6.
21. Ferreira, R.T.L.; Amatte, I.C.; Dutra, T.A.; Burger, D. Experimental characterization and micrography of 3D printed PLA and PLA reinforced with short carbon fibers. *Compos. Part B Eng.* **2017**, *124*, 88–100. [CrossRef]
22. Shofner, M.; Lozano, K.; Rodriguez-Macias, F.; Barrera, E. Nanofiber-Reinforced polymers prepared by fused deposition modeling. *J. Appl. Polym. Sci.* **2003**, *89*, 3081–3090. [CrossRef]
23. Lanzotti, A.; Pei, E.; Grasso, M.; Staiano, G.; Martorelli, M. The impact of process parameters on mechanical properties of parts fabricated in PLA with an open-source 3-D printer. *Rapid Prototyp. J.* **2015**, *21*, 604–617. [CrossRef]
24. Cantrell, J.; Rohde, S.; Damiani, D.; Gurnani, R.; DiSandro, L.; Anton, J.; Young, A.; Jerez, A.; Steinbach, D.; Kroese, C.; et al. Experimental characterization of the mechanical properties of 3D-printed ABS and polycarbonate parts. *Rapid Prototyp. J.* **2017**. [CrossRef]
25. Perez, A.R.T.; Roberson, D.A.; Wicker, R.B. Fracture surface analysis of 3D-printed tensile specimens of novel ABS-based materials. *J. Fail. Anal. Prev.* **2014**, *14*, 343–353. [CrossRef]
26. Onwubolu, G.C.; Rayegani, F. Characterization and optimization of mechanical properties of ABS parts manufactured by the fused deposition modelling process. *Int. J. Manuf. Eng.* **2014**, *2014*. [CrossRef]
27. Christiyan, K.J.; Chandrasekhar, U.; Venkateswarlu, K. A study on the influence of process parameters on the Mechanical Properties of 3D printed ABS composite. *Proc. IOP Conf. Ser. Mater. Sci. Eng.* **2016**, *114*, 012109. [CrossRef]
28. Walter, R.; Friedrich, K.; Gurka, M. Characterization of mechanical properties of additively manufactured polymers and composites. *AIP Conf. Proc.* **2018**, 020033. [CrossRef]
29. Blok, L.G.; Longana, M.L.; Yu, H.; Woods, B.K. An investigation into 3D printing of fibre reinforced thermoplastic composites. *Addit. Manuf.* **2018**, *22*, 176–186. [CrossRef]
30. Nazan, M.A.; Ramli, F.R.; Alkahari, M.R.; Sudin, M.N.; Abdullah, M. Process parameter optimization of 3D printer using response surface method. *ARPN J. Eng. Appl. Sci.* **2017**, *12*, 2291–2296.
31. Liao, G.; Li, Z.; Cheng, Y.; Xu, D.; Zhu, D.; Jiang, S.; Guo, J.; Chen, X.; Xu, G.; Zhu, Y. Properties of oriented carbon fiber/polyamide 12 composite parts fabricated by fused deposition modeling. *Mater. Des.* **2018**, *139*, 283–292. [CrossRef]
32. Banerjee, S.S.; Burbine, S.; Kodihalli Shivaprakash, N.; Mead, J. 3D-printable PP/SEBS thermoplastic elastomeric blends: Preparation and properties. *Polymers* **2019**, *11*, 347. [CrossRef] [PubMed]
33. Gebisa, A.W.; Lemu, H.G. Influence of 3D Printing FDM Process Parameters on Tensile Property of ULTEM 9085. *Procedia Manuf.* **2019**, *30*, 331–338. [CrossRef]
34. Li, N.; Li, Y.; Liu, S. Rapid prototyping of continuous carbon fiber reinforced polylactic acid composites by 3D printing. *J. Mater. Process. Technol.* **2016**, *238*, 218–225. [CrossRef]
35. Tian, X.; Liu, T.; Yang, C.; Wang, Q.; Li, D. Interface and performance of 3D printed continuous carbon fiber reinforced PLA composites. *Compos. Part A Appl. Sci. Manuf.* **2016**, *88*, 198–205. [CrossRef]
36. Fasel, U.; Keidel, D.; Baumann, L.; Cavolina, G.; Eichenhofer, M.; Ermanni, P. Composite additive manufacturing of morphing aerospace structures. *Manuf. Lett.* **2020**, *23*, 85–88. [CrossRef]
37. Hou, Z.; Tian, X.; Zhang, J.; Li, D. 3D printed continuous fibre reinforced composite corrugated structure. *Compos. Struct.* **2018**, *184*, 1005–1010. [CrossRef]
38. Tekinalp, H.L.; Kunc, V.; Velez-Garcia, G.M.; Duty, C.E.; Love, L.J.; Naskar, A.K.; Blue, C.A.; Ozcan, S. Highly oriented carbon fiber—Polymer composites via additive manufacturing. *Compos. Sci. Technol.* **2014**, *105*, 144–150. [CrossRef]

39. Ning, F.; Cong, W.; Hu, Y.; Wang, H. Additive manufacturing of carbon fiber-reinforced plastic composites using fused deposition modeling: Effects of process parameters on tensile properties. *J. Compos. Mater.* **2017**, *51*, 451–462. [CrossRef]
40. Brenken, B.; Barocio, E.; Favaloro, A.; Kunc, V.; Pipes, R.B. Fused filament fabrication of fiber-reinforced polymers: A review. *Addit. Manuf.* **2018**, *21*, 1–16. [CrossRef]
41. Ning, F.; Cong, W.; Qiu, J.; Wei, J.; Wang, S. Additive manufacturing of carbon fiber reinforced thermoplastic composites using fused deposition modeling. *Compos. Part B Eng.* **2015**, *80*, 369–378. [CrossRef]
42. Turner, B.N.; Strong, R.; Gold, S.A. A review of melt extrusion additive manufacturing processes: I. Process design and modeling. *Rapid Prototyp. J.* **2014**, *20*, 192–204. [CrossRef]
43. Song, Y.; Li, Y.; Song, W.; Yee, K.; Lee, K.-Y.; Tagarielli, V.L. Measurements of the mechanical response of unidirectional 3D-printed PLA. *Mater. Des.* **2017**, *123*, 154–164. [CrossRef]
44. Sun, Q.; Rizvi, G.; Bellehumeur, C.; Gu, P. Effect of processing conditions on the bonding quality of FDM polymer filaments. *Rapid Prototyp. J.* **2008**, *14*, 72–80. [CrossRef]
45. Smith, W.C.; Dean, R.W. Structural characteristics of fused deposition modeling polycarbonate material. *Polym. Test.* **2013**, *32*, 1306–1312. [CrossRef]
46. Durgun, I.; Ertan, R. Experimental investigation of FDM process for improvement of mechanical properties and production cost. *Rapid Prototyp. J.* **2014**. [CrossRef]
47. Duty, C.E.; Drye, T.; Franc, A. *Material Development for Tooling Applications Using Big Area Additive Manufacturing (BAAM)*; Oak Ridge National Lab. (ORNL): Oak Ridge, TN, USA; Manufacturing Demonstration Facility (MDF): Knoxville, TN, USA, 2015.
48. Duty, C.E.; Kunc, V.; Compton, B.; Post, B.; Erdman, D.; Smith, R.; Lind, R.; Lloyd, P.; Love, L. Structure and mechanical behavior of Big Area Additive Manufacturing (BAAM) materials. *Rapid Prototyp. J.* **2017**. [CrossRef]
49. Love, L.J.; Kunc, V.; Rios, O.; Duty, C.E.; Elliott, A.M.; Post, B.K.; Smith, R.J.; Blue, C.A. The importance of carbon fiber to polymer additive manufacturing. *J. Mater. Res.* **2014**, *29*, 1893–1898. [CrossRef]
50. Ding, Q.; Li, X.; Zhang, D.; Zhao, G.; Sun, Z. Anisotropy of poly (lactic acid)/carbon fiber composites prepared by fused deposition modeling. *J. Appl. Polym. Sci.* **2020**, *137*, 48786. [CrossRef]
51. Wang, K.; Li, S.; Rao, Y.; Wu, Y.; Peng, Y.; Yao, S.; Zhang, H.; Ahzi, S. Flexure behaviors of ABS-based composites containing carbon and Kevlar fibers by material extrusion 3D printing. *Polymers* **2019**, *11*, 1878. [CrossRef]
52. Chacón, J.M.; Caminero, M.A.; Núñez, P.J.; García-Plaza, E.; García-Moreno, I.; Reverte, J.M. Additive manufacturing of continuous fibre reinforced thermoplastic composites using fused deposition modelling: Effect of process parameters on mechanical properties. *Compos. Sci. Technol.* **2019**, *181*, 107688. [CrossRef]
53. Caminero, M.; Chacón, J.M.; García-Moreno, I.; Rodríguez, G.P. Impact damage resistance of 3D printed continuous fibre reinforced thermoplastic composites using fused deposition modelling. *Compos. Part B Eng.* **2018**, *148*, 93–103. [CrossRef]
54. Hill, N.; Haghi, M. Deposition direction-dependent failure criteria for fused deposition modeling polycarbonate. *Rapid Prototyp. J.* **2014**, *20*, 221–227. [CrossRef]
55. Carneiro, O.S.; Silva, A.; Gomes, R. Fused deposition modeling with polypropylene. *Mater. Des.* **2015**, *83*, 768–776. [CrossRef]
56. Dawoud, M.; Taha, I.; Ebeid, S.J. Mechanical behaviour of ABS: An experimental study using FDM and injection moulding techniques. *J. Manuf. Process.* **2016**, *21*, 39–45. [CrossRef]
57. Hossain, M.S.; Ramos, J.; Espalin, D.; Perez, M.; Wicker, R. Improving tensile mechanical properties of FDM-manufactured specimens via modifying build parameters. In Proceedings of the International Solid Freeform Fabrication Symposium: An Additive Manufacturing Conference, Austin, TX, USA, 12–14 August 2019; pp. 380–392.
58. Papon, M.E.A.; Haque, A.; Ma, R.S. Effect of nozzle geometry on melt flow simulation and structural property of thermoplastic nanocomposites in fused deposition modeling. In Proceedings of the Thirty-Second Technical Conference, American Society for Composites, West Lafayette, IN, USA, 23–25 October 2017.
59. Comminal, R.; Serdeczny, M.; Pedersen, D.; Spangenberg, J. Numerical modeling of the material deposition and contouring precision in fused deposition modeling. In Proceedings of the 29th Annual International Solid Freeform Fabrication Symposium, Austin, TX, USA, 13–15 August 2018; pp. 13–15.
60. Comminal, R.; Serdeczny, M.P.; Pedersen, D.B.; Spangenberg, J. Motion planning and numerical simulation of material deposition at corners in extrusion additive manufacturing. *Addit. Manuf.* **2019**, *29*, 100753. [CrossRef]
61. Namiki, M.; Ueda, M.; Todoroki, A.; Hirano, Y. 3D printing of continuous fiber reinforced plastic. In Proceedings of the SAMPE 2014, International SAMPE Symposium and Exhibition, Seattle, WA, USA, 2–5 June 2014.
62. Anitha, R.; Arunachalam, S.; Radhakrishnan, P. Critical parameters influencing the quality of prototypes in fused deposition modelling. *J. Mater. Process. Technol.* **2001**, *118*, 385–388. [CrossRef]
63. Croccolo, D.; De Agostinis, M.; Olmi, G. Experimental characterization and analytical modelling of the mechanical behaviour of fused deposition processed parts made of ABS-M30. *Comput. Mater. Sci.* **2013**, *79*, 506–518. [CrossRef]
64. Verdejo de Toro, E.; Coello Sobrino, J.; Martínez Martínez, A.; Miguel Eguía, V.; Ayllón Pérez, J. Investigation of a Short Carbon Fibre-Reinforced Polyamide and Comparison of Two Manufacturing Processes: Fused Deposition Modelling (FDM) and Polymer Injection Moulding (PIM). *Materials* **2020**, *13*, 672. [CrossRef]
65. Yasa, E.; Ersoy, K. Dimensional Accuracy and Mechanical Properties of Chopped Carbon Reinforced Polymers Produced by Material Extrusion Additive Manufacturing. *Materials* **2019**, *12*, 3885. [CrossRef]

66. Yasa, E. Anisotropic impact toughnness of chopped carbon fiber reinforced nylon fabricated by material-extrusion-based additive manufacturing. *Anadolu Univ. Sci. Technol. A Appl. Sci. Eng.* **2019**, *20*. [CrossRef]
67. Aworinde, A.K.; Adeosun, S.O.; Oyawale, F.A.; Akinlabi, E.T.; Akinlabi, S.A. Parametric Effects of Fused Deposition Modelling on the Mechanical Properties of Polylactide Composites: A Review. *J. Phys. Conf. Ser.* **2019**, 022060. [CrossRef]
68. MarkForged. MarkForged Visual Troubleshooting Guide. Available online: https://support.markforged.com/hc/en-us/articles/205927119-MarkForged-Visual-Troubleshooting-Guide (accessed on 25 March 2020).
69. Sukindar, N.A.; Ariffin, M.K.A.; Baharudin, B.H.T.; Jaafar, C.N.A.; Ismail, M.I.S. Analyzing the effect of nozzle diameter in fused deposition modeling for extruding polylactic acid using open source 3D printing. *J. Teknol.* **2016**, *78*. [CrossRef]
70. Blok, L.G.; Longana, M.L.; Woods, B.K.S. Fabrication and characterisation of aligned discontinuous carbon fibre reinforced thermoplastics for automated manufacture. *Materials* **2020**, *13*, 4671. [CrossRef] [PubMed]
71. 3D Matter. What is the Best Type of Plastic for My 3D Printing Application? Available online: https://my3dmatter.com/what-is-the-best-type-of-plastic-for-my-3d-printing-application/ (accessed on 11 March 2020).
72. 3D Matter. FDM 3D Printing Materials Compared. Available online: https://www.3dhubs.com/knowledge-base/fdm-3d-printing-materials-compared/ (accessed on 20 March 2020).
73. Wilson, A. 1—The formation of dry, wet, spunlaid and other types of nonwovens. *Appl. Nonwovens Tech. Text.* **2010**, 3–17. [CrossRef]
74. Zhuo, P.; Li, S.; Ashcroft, I.; Jones, A.; Pu, J. 3D printing of continuous fibre reinforced thermoplastic composites. In Proceedings of the 21st International Conference on Composite Materials, ICCM21, ID, Xi'an, China, 20–25 August 2017.
75. Al Abadi, H.; Thai, H.-T.; Paton-Cole, V.; Patel, V.I. Elastic properties of 3D printed fibre-reinforced structures. *Compos. Struct.* **2018**, *193*, 8–18. [CrossRef]
76. Matsuzaki, R.; Ueda, M.; Namiki, M.; Jeong, T.-K.; Asahara, H.; Horiguchi, K.; Nakamura, T.; Todoroki, A.; Hirano, Y. Three-Dimensional printing of continuous-fiber composites by in-nozzle impregnation. *Sci. Rep.* **2016**, *6*, 23058. [CrossRef] [PubMed]
77. Heller, B.P.; Smith, D.E.; Jack, D.A. Effects of extrudate swell and nozzle geometry on fiber orientation in Fused Filament Fabrication nozzle flow. *Addit. Manuf.* **2016**, *12*, 252–264. [CrossRef]
78. Mulholland, T.; Goris, S.; Boxleitner, J.; Osswald, T.; Rudolph, N. Fiber Orientation Effects in Fused Filament Fabrication of Air-Cooled Heat Exchangers. *JOM* **2018**, *70*, 298–302. [CrossRef]
79. Hofstätter, T.; Gutmann, I.W.; Koch, T.; Pedersen, D.B.; Tosello, G.; Heinz, G.; Hansen, N. Distribution and orientation of carbon fibers in polylactic acid parts produced by fused deposition modeling. In Proceedings of the ASPE Summer Topical Meeting, Raleigh, NC, USA, 27–30 June 2016.
80. Yu, H.; Potter, K.D.; Wisnom, M.R. A novel manufacturing method for aligned discontinuous fibre composites (High Performance-Discontinuous Fibre method). *Compos. Part A Appl. Sci. Manuf.* **2014**, *65*, 175–185. [CrossRef]
81. Such, M.; Ward, C.; Potter, K. Aligned discontinuous fibre composites: A short history. *J. Multifunct. Compos.* **2014**, *2*, 155–168. [CrossRef]
82. Folgar, F.; Tucker, C.L., III. Orientation behavior of fibers in concentrated suspensions. *J. Reinf. Plast. Compos.* **1984**, *3*, 98–119. [CrossRef]
83. Cicala, G.; Giordano, D.; Tosto, C.; Filippone, G.; Recca, A.; Blanco, I. Polylactide (PLA) filaments a biobased solution for additive manufacturing: Correlating rheology and thermomechanical properties with printing quality. *Materials* **2018**, *11*, 1191. [CrossRef] [PubMed]
84. Dickson, A.N.; Barry, J.N.; McDonnell, K.A.; Dowling, D.P. Fabrication of continuous carbon, glass and Kevlar fibre reinforced polymer composites using additive manufacturing. *Addit. Manuf.* **2017**, *16*, 146–152. [CrossRef]
85. Mohammadizadeh, M.; Imeri, A.; Fidan, I.; Elkelany, M. 3D printed fiber reinforced polymer composites-Structural analysis. *Compos. Part B Eng.* **2019**, *175*, 107112. [CrossRef]
86. Van Der Klift, F.; Koga, Y.; Todoroki, A.; Ueda, M.; Hirano, Y.; Matsuzaki, R. 3D printing of continuous carbon fibre reinforced thermo-plastic (CFRTP) tensile test specimens. *Open J. Compos. Mater.* **2016**, *6*, 18–27. [CrossRef]
87. Tey, J.; Ding, W.; Yeo, W.; King, Y.; Saw, L. 3D printing of continuous kevlar reinforced polymer composite through coextrusion method. *IOP Conf. Ser. Earth Environ. Sci.* **2020**, *463*, 012091. [CrossRef]
88. Ultimaker. Technical Data Sheet PLA. Available online: https://ultimaker.com/download/74599/UM180821%20TDS%20PLA%20RB%20V10.pdf (accessed on 15 March 2020).
89. Ultimaker. Technical Data Sheet ABS. Available online: https://ultimaker.com/download/74640/UM180821%20TDS%20ABS%20RB%20V11.pdf (accessed on 15 March 2020).
90. Simplify3D. Filament Properties Table. Available online: https://www.simplify3d.com/support/materials-guide/properties-table/ (accessed on 15 March 2020).
91. Giang, K. PLA vs. ABS: What's the Difference? Available online: https://www.3dhubs.com/knowledge-base/pla-vs-abs-whats-difference/ (accessed on 16 March 2020).
92. Ultimaker. Technical Data Sheet PP. Available online: https://ultimaker.com/download/74977/UM180821%20TDS%20PP%20RB%20V11.pdf (accessed on 15 March 2020).
93. SD3D Printing. Technical Data Sheet PLA. Available online: https://www.sd3d.com/wp-content/uploads/2017/06/MaterialTDS-PLA_01.pdf (accessed on 15 March 2020).

94. Rogers, T. Everything You Need to Know About ABS Plastic. Available online: https://www.creativemechanisms.com/blog/everything-you-need-to-know-about-abs-plastic (accessed on 18 February 2020).
95. Engineering ToolBox. Young's Modulus—Tensile and Yield Strength for Common Materials. Available online: https://www.engineeringtoolbox.com/young-modulus-d_417.html (accessed on 1 May 2020).
96. MatWeb, L. Overview of Materials for Polylactic Acid (PLA) Biopolymer. Available online: http://www.matweb.com/search/DataSheet.aspx?MatGUID=ab96a4c0655c4018a8785ac4031b9278 (accessed on 1 May 2020).
97. O'Neal, B. Navigating through the Selection of 3D Printing Materials: Know Your Strengths! Available online: https://3dprint.com/42417/3d-printing-material-strengths/ (accessed on 6 March 2020).
98. Designerdata. PP. Available online: https://designerdata.nl/materials/plastics/thermo-plastics/polypropylene-(cop.) (accessed on 1 May 2020).
99. Chilson, L. Comparison of Typical 3D Printing Materials. Available online: http://2015.igem.org/wiki/images/2/24/CamJIC-Specs-Strength.pdf (accessed on 16 February 2020).
100. Vexma Technologies. Polycarbonate (PC). Available online: https://vexmatech.com/PC-polycarbonate-FDM-technology-3dprinting-material.html (accessed on 8 March 2020).
101. BCN3D. Unlock a Wide Range of Applications with the Revamped Industrial-Grade BCN3D Filaments Portfolio. Available online: https://www.bcn3d.com/revamped-industrial-grade-bcn3d-basf-mitsubishi-filaments-portfolio/ (accessed on 16 March 2020).
102. 3D4Maker.com. PEI Filament Ultem 1010. Available online: https://www.multi-3dprint.nl/images/3d4makers/TDS_PEI_ULTEM_1010.pdf (accessed on 10 February 2020).
103. Ultimaker. Technical Data Sheet PC. Available online: https://ultimaker.com/download/74975/UM180821%20TDS%20PC%20RB%20V11.pdf (accessed on 20 March 2020).
104. Ultimaker. Technical Data Sheet Nylon. Available online: https://ultimaker.com/download/74598/UM180821%20TDS%20Nylon%20RB%20V10.pdf (accessed on 1 May 2020).
105. Stratasys. ULTEM™ 1010 Resin. Available online: https://www.stratasys.com/materials/search/ultem1010 (accessed on 28 March 2020).
106. Javelin. PC (Polycarbonate). Available online: https://www.javelin-tech.com/3d/stratasys-materials/pc/ (accessed on 1 May 2020).
107. Fillamentum. Technical Data Sheet Nylon FX256. Available online: https://www.materialpro3d.cz/user/related_files/fillamentum_nylon_fx256_-_technical_data_sheet.pdf (accessed on 1 May 2020).
108. Sabic. ULTEM™ RESIN. Available online: https://www.sabic.com/en/products/specialties/ultem-resins/ultem-resin (accessed on 1 May 2020).
109. Stratasys. FORTUS PC (Polycarbonate). Available online: http://producto3d.com/wp-content/uploads/2018/01/FDM_PCPropertiesReport.pdf (accessed on 1 May 2020).
110. Fast Radius. Know Your Materials: PA 12. Available online: https://www.fastradius.com/resources/polyamide-12/ (accessed on 18 March 2020).
111. 3dgence. PEEK Filament. Available online: http://support.3dgence.com/twoje-pliki/downloader/1352/TDS_PEEK_Filament_1.pdf (accessed on 20 November 2020).
112. Theplasticshop. Ketron®1000 PEEK. Available online: https://www.theplasticshop.co.uk/plastic_technical_data_sheets/peek_1000_technical_data_sheet.pdf (accessed on 23 March 2020).
113. CURBELL Plastics. PEEK Strong, Stiff Plastic with Outstanding Chemical Resistance; Performs over a Wide Range of Temps. Available online: https://www.curbellplastics.com/Research-Solutions/Technical-Resources/Technical-Resources/PEEK-Data-Sheet (accessed on 28 March 2020).